UNIVERSITY OF CALIFORNIA SAN DIEGO

O-GlcNAcylation dynamics in the brain

I. Brain region-specific characterization of nutrient-driven O-GlcNAcylation

II. The role of O-GlcNAc Transferase in parvalbumin interneurons

A Thesis submitted in partial satisfaction of the requirements for the degree

Master of Science in Biology

by

Norah Al-Azzam

Committee in charge:

Professor Gulcin Pekkurnaz, Chair
Professor Stacey Glasgow
Professor Yishi Jin

2020

The thesis of Norah Al-azzam is approved, and it is acceptable in quality and form for publication on microfilm and electronically:

_____

_____

_____
Chair

University of California San Diego

2020

DEDICATIONS

I would like to dedicate this thesis to my supervisor who was the guiding light every step of the way as I researched for this thesis. I would like to also dedicate this to my family who supported me through pursuing higher education.

TABLE OF CONTENTS

LIST OF FIGURES AND TABLES

ACKNOWLEDGMENTS

I would like to acknowledge Professor Gulcin Pekkurnaz for her support as the chair of my committee. Through multiple drafts, her guidance has proved to be invaluable. I want to thank my committee members, Dr.Glasgow and Dr. Jin, for their support as well.

Chapter 2 is co- authored with Roberts, Amanda and De-lugo, Arlina. The thesis author, Norah Al-Azzam, was the primary and first author of this chapter.

ABSTRACT OF THE THESIS

O-GlcNAcylation Dynamics in the Brain

by

Norah Al-Azzam

Master of Science in Biology

University of California San Diego, 2020

Professor Gulcin Pekkurnaz, Chair

The role of post-translational modifications in the brain such as phosphorylation and ubiquitination have been well studied. However, the role of O-GlcNAcylation in distinct subpopulations of neurons remains unknown. This post-translational modification is an addition of single sugar moiety O-GlcNAc, derived from glucose metabolism, to serine or threonine residue of proteins. O-GlcNAcylation is catalyzed by O-GlcNAc transferase (OGT), a highly expressed metabolic sensor enzyme in the brain, shown to be a gatekeeper for neuronal function and health. Here, we investigated the role of OGT and O-GlcNAc dynamics in the brain. First, we demonstrated under the fasted state, brain regions such as the paraventricular nucleus of hypothalamus, cortex and cerebellum, have significant reduction in O-GlcNAc levels. While the hippocampus regions, CA3 and dentate gyrus, have increased levels of O-GlcNAcylation. Then in order to investigate the role of O-GlcNAcylation in Parvalbumin-positive inhibitory interneurons (PV), we generated a PV-specific-OGT knockout mouse line (PV.OGTKO). Our detailed behavioral and histological analysis indicated that loss of OGT in PV neurons leads to lower survival rates, motor defects, and loss of PV neurons. Overall, our results suggest the OGT plays crucial role in PV neuronal health and survival.

CHAPTER 1

Brain region-specific characterization of nutrient-driven O-GlcNAcylation

Glucose is the main energy source of the mammalian brain. Brain functions such as information processing, memory formation, and emotions are closely linked to glucose levels and the efficiency of its metabolism in the brain. Highly active brain regions require more energy and consume more glucose. Hence, the metabolic rate of glucose displays heterogeneity between different brain regions. Metabolic sensor enzymes play a critical role in maintaining energy homeostasis in the brain by sensing nutrient availability and tailoring intracellular signaling pathways accordingly. One of the highly expressed metabolic sensor enzymes in the brain is O-GlcNAc Transferase (OGT). OGT catalyzes addition of single sugar moiety N-Acetylglucosamine (O-GlcNAc), a post-translational modification (PTM), through the on serine or threonine residues of intracellular proteins. Although thousands of neuronal proteins are identified to be O-GlcNAc modified, little is known about its distribution within the different brain regions. Here we have investigated the spatiotemporal distribution of O-GlcNAcylation in mice brains under different metabolic conditions such as hypo- and hyperglycemia. By using an O-GlcNAc specific antibody, our immunohistochemical analysis revealed unique O-GlcNAcylation patterns in hippocampus, cerebellum, cortex, and hypothalamus under different satiety states in mice. By uncovering the O-GlcNAcylation dynamics that change in specific brain regions and nutrient states, our goal is to provide key insights into the regulatory role of OGT in the brain.

INTRODUCTION

The brain weighs 2% of the human body, yet it consumes an average of 20% of the total energy generated in the body [1,2]. Glucose is the main fuel for the brain [2]. For the brain to function efficiently at a high metabolic rate, metabolic sensor enzymes are required to maintain energy homeostasis based on nutrient availability [1,2]. One important metabolic sensing mechanism is post-translational modification (PTM) called O-GlcNAcylation, catalyzed by the enzyme O-GlcNAc Transferase (OGT). O-GlcNAc is derived from a single sugar moiety through glucose metabolism, which can then be covalently added to serine and threonine residues on proteins [3,4]. While the majority of glucose is used for glycolysis about 2-5% enters the hexosamine pathway (HBP) to derive UDP-GlcNAc, which is a donor substrate for O-GlcNAc transferase (OGT) [4]. OGT uses this nucleotide sugar to glycosylate nuclear, cytoplasmic and mitochondrial proteins [4]. The HBP pathway is an important component of metabolic sensing in the nervous system. OGT activity is regulated by the intracellular UDP-GlcNAc level and metabolic hormones like insulin [5]. Alterations in HBP pathway may induce insulin resistance [6,7].

The O-GlcNAc-modified proteins (> 4,000 proteins) the key regulators in gene expression, epigenetics, translation, protein degradation, signal transduction, mitochondrial bioenergetics, cell cycling, and protein localization [3,4]. OGT is a highly expressed enzyme in the brain, and important for neuronal function [5]. O-GlcNAc cycling in neurons regulate synaptic activity, play critical role in neuronal signaling, and dynamically change organelle trafficking [5,8].

Dysregulation of OGT activity or O-GlcNAcylation level can lead to metabolic disorders [9-12]. High levels of OGT have been observed in diabetic patients, and OGT genetic mutations have been demonstrated to be prevalent in members of the Mexican American population suffering from type 2 diabetes (T2D) [13]. Similar to what is observed in T2D, low OGT expression/activity in neurons has been linked to late-onset of Alzheimer's disease (AD), where both global and specific reduction of O-GlcNAcylation on proteins is observed [9-10]. Furthermore, major risks of developing AD are associated with insulin signaling and neuronal internal metabolism signaling pathways for processing glucose [10-12]. Additionally, many glucose transporters in neurons such as GLUT1 and GLUT3 are post-translationally modified by O-GlcNAc and are decreased in activity of the AD brain [1,9-12].

Similar to tau hyper-phosphorylation and protein aggregation, tau hypo-O-GlcNAcylation has been detected in AD mouse models as well as in human AD tissue samples as a consequence of decreased brain glucose metabolism [11]. Increased phosphorylation leads to reduction in tau O-GlcNAcylation because both modifications compete for the same serine and threonine residues [11]. Tau O-GlcNAcylation is regulated by intraneuronal glucose levels [11,12,14]. 48 hours of fasting *in vivo* causes time-dependent decrease in tau O-GlcNAcylation levels and hyperphosphorylation, in the hippocampus, which is the defining feature brain-region specific glucose hypometabolism in AD [14].

Impaired glucose metabolism, as in AD and T2D, alters overall protein O-GlcNAcylation in the brain and other tissues. O-GlcNAcylation also regulate feeding circuitry [15]. The cell-type specific knock-out of OGT in excitatory neurons increases

food consumption in mice and leads to weight gain due to loss of O-GlcNAcylation particularly in the paraventricular nucleus (PVN) region of the brain [15]. This region is found near the third ventricle, controlling pituitary-adrenocortical activity in response to stress, body fluid homeostasis, thyroid hormone secretion, and food intake. Upon 24 hours of fasting causes reduction O-GlcNAcylation levels in excitatory neurons of the PVN [15]. However, this study failed to show levels of O-GlcNAcylation upon refeeding and whether any other brain regions are affected upon fasting.

Here, we aimed to investigate the spatiotemporal distribution of O-GlcNAcylation in mice brains under different nutrient states (i.e. hypoglycemia, normoglycemia). By using an O-GlcNAc-specific antibody, we conducted an immunohistochemical analysis from the fixed brain tissue to reveal unique O-GlcNAcylation patterns in the hippocampus, cerebellum, cortex, and hypothalamus under different satiety states in mice. The future research goal is to analyze the diabetic and neurodegenerative brain to evaluate O-GlcNAc distribution and potential anomalies in different brain regions under different satiety states. These findings may provide key insights into the regulatory role of OGT in T2D and neurological disorders.

RESULTS

Fasting-induced reduction of O-GlcNAcylation in the PVN region

We first evaluated whether the fasting of mice indeed induced a decreased level of O-GlcNAc in the different brain regions. First, I have established fasting/refeeding paradigm as described in Figure 1B. Glucose and O-GlcNAc levels have a correlative relationship; when extracellular glucose goes up, so does O-GlcNAc (Fig. 1A). The experimental groups included a first group fed ad libitum (*ad lib)* a second group fasted for 24 hours, and a third group which was fasted for 24 hours and refed for the next 24 hours, wherein, in the end, the mice were sacrificed (Fig. 1B). For each group the mice were sacrificed in a 10-minute window, shortening possibilities for blood glucose level changes. Furthermore, to confirm whether mice were properly fasted and refed, blood glucose level was measured (Fig. 1C).

The monoclonal RL2 antibody was used to investigate O-GlcNAc levels in the soma of neurons in the Paraventricular Nucleus of Hypothalamus (PVN), localized close to the third ventricle (V3), (Fig. 2A) under the fasting/refeeding states of mice. The role of this region is to control pituitary-adrenocortical activity in response to stress, body fluid homeostasis, thyroid hormone secretion, and food intake. Three 8-week-old male mice were used in each individual experiment for PVN region immunostaining, which was repeated three times (n=3). To measure neuron-specific O-GlcNAc intensity, we stained with a NeuN antibody together with O-GlcNAc antibody and DAPI. Our analysis revealed overall reduction of PVN O-GlcNAcylation after 24 hours fasting period, which was recovered globally upon re-feeding of mice after 24 hours (Fig. 2B-C).

Fasting-induced reduction of O-GlcNAcylation in Cerebral Cortex

The cerebral cortex consumes 50% of the generated energy in the brain, making the cortex the most energy demanding region of the brain [16]. The feeding/fasting/refeeding experiment was performed as described above, cortical tissue was evaluated for O-GlcNAc signal. Under fasting conditions, more than 50% of O-GlcNAcylation is reduced in cortical neurons (Fig. 3C). Our results suggests that O-GlcNAc cycling is sensitive to blood glucose level in cortical neurons.

Fasting-induced increase of O-GlcNAcylation in hippocampal neurons

Previous studies have shown a decrease in O-GlcNAcylation in hippocampal tissue extractions using western blot staining after 24 hours of fasting in mice [17]. However, later in this study they only showed an immunostaining of tau phosphorylation, not O-GlcNAc level of the dentate gyrus (DG) and cornu ammonis 3 (CA3). When we performed our feeding/fasting/refeeding experiment to evaluate O-GlcNAc level in the hippocampus, O-GlcNAc levels rose in the DG and CA3 upon fasting and refeeding (Fig. 4B and Fig. 5B). We have shown the strongest O-GlcNAc intensity and dense distribution in all pyramidal neurons and mossy fibers in the stratum lucidum in CA3 (Fig. 4C and 5C). After fasting for 24 hours, re-feeding for 24 hours, there increased staining with Rl2 antibody compared to *Adlib* and fasted mice (SFig. 1A and SFig. 1B). Unlike other brain regions evaluated, why fasting increases O-GlcNAc level in the hippocampus requires further investigation.

Reduced in O-GlcNAcylation at Purkinje layer upon fasting

We have observed a decrease in the O-GlcNAcylation level in the purkinje cell layer of the cerebellum, especially at ansiform lobule curs 1(AnCR1) upon fasting. In the

cerebellum Purkinje cells use 62 times more energy than cells in the granular layer cells [16]. Purkinje cells have more glucose transporters compared to other excitatory and inhibitory cells in the brain and high energy demand.[16]. Therefore, fasting-depending reduction of O-GlcNAcylation levels (Fig. 6B-C) indicates the critical metabolic sensing role of OGT in this brain region, and requires further investigation.

DISCUSSION

Many nuclear and cytoplasmic proteins are modified by O-GlcNAc. This rapid and highly dynamic cytoplasmic, nuclear and mitochondrial glycosylation process regulates signal transduction, transcription, translation, and proteasomal degradation [6]. Dysregulation in O-GlcNAc cycling is associated with diabetes and aging disorders [6,9-10]. Since O-GlcNAcylation levels in neurons are regulated by intraneuronal glucose metabolism, O-GlcNAc plays a nutrient sensing role [5-6]. The glucose uptake system, therefore O-GlcNAcylation, in neurons is highly integrated into the metabolic rate and synaptic activity.

In this study, we assessed how brain O-GlcNAcylation dynamics are altered in different brain regions upon fasting/feeding in mice. We took advantage of the fact that the concentration of extracellular glucose in the brain changes in parallel with blood glucose level during fasting and feeding cycles [18]. Our results suggest that different brain regions and sub-neuronal-populations in response to brain glucose uptake/metabolism influx have different O-GlcNAcylation levels.

Previous studies have indicated PVN as the OGT-activity sensitive brain region [15,19]. OGT regulates excitatory synaptic input in the PVN, where mostly vGlut2-positive excitatory neurons such as agouti-related protein (AgRP), neuropeptide Y (NYP), and proopiomelanocortin (POMC) have critical roles in maintaining energy homogenization and glucose metabolism. In addition to PVN, our data indicates that OGT activity in other brain regions including cortex, cerebellum, and hippocampus seemed to be coupled with nutrient availability.

In our study, we sought to determine which regions are more sensitive to nutrient availability. As hypothesized after fasting O-GlcNAcylation levels should go back to *ad lib* levels however, this was not in the case for some brain regions such as the hippocampus. In this region, we are the first to show that upon fasting O-GlcNAc levels rise in the CA3 and DG (Fig. 4B and Fig. 5B).

This present study has provided the new insights into the molecular mechanism by which hypoglycemia and hyperglycemia can affect O-GlcNAc dynamics in different brain regions. We have found that low brain glucose uptake and metabolism during fasting results in a decreased O-GlcNAcylation in the cerebellum, cortex, and hypothalamus. In contrast, at low glucose levels hippocampal O-GlcNAcylation is increased. The systematic analysis of O-GlcNAc distribution as a function of blood glucose level will be a landmark study because it will determine which areas to target for knock-out studies of OGT to investigate vulnerable glucose-sensing neurons. The feeding/fasting/refeeding protocol I established will also be used for biochemical assays by other lab members to carry out.

FIGURES

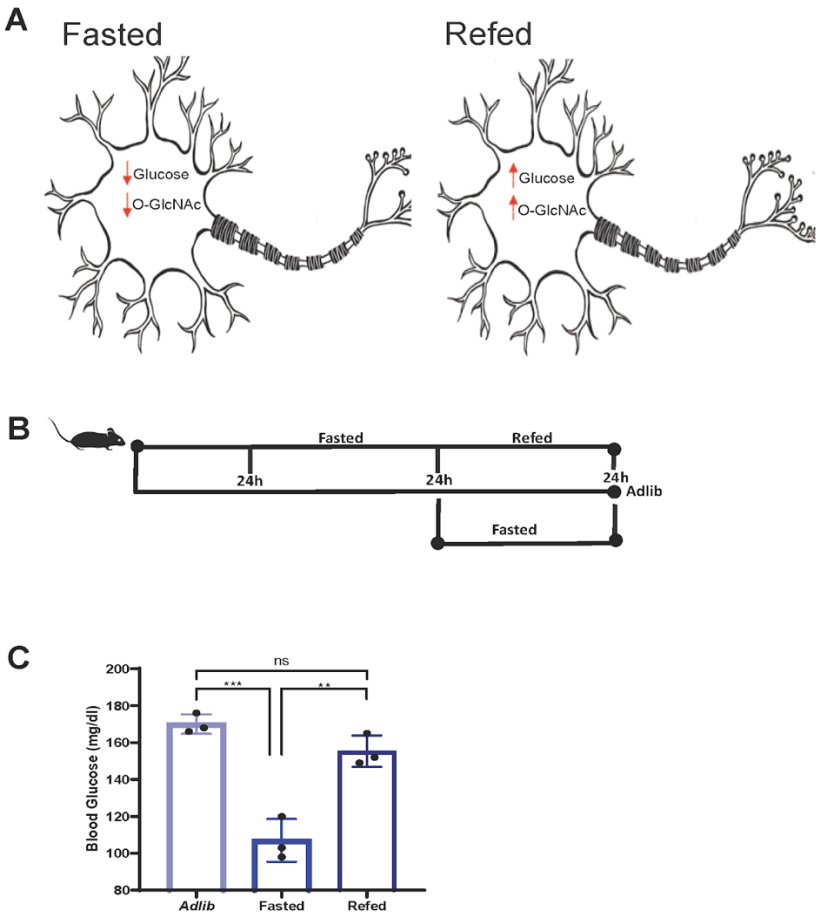

Figure 1.1: Fasting/Feeding- Dependent Blood Glucose Level Change (A) Neuron Scheme Summarizing Of Feeding/Fasting Dependent O-Glcnac Levels Changes. (B) Experimental Design For Changing Blood Glucose Levels, Fasting, Re-Feeding, And *Adlib* Groups. (C) The Blood Glucose Level Measurements Upon Feeding/Fasting From The Mice Used For O-Glcnacylation Levels Comparisons. Data Was Analyzed With Tukey's Multiple Comparisons Tests (N=3), ***P=0.0003, **P=0.0013.

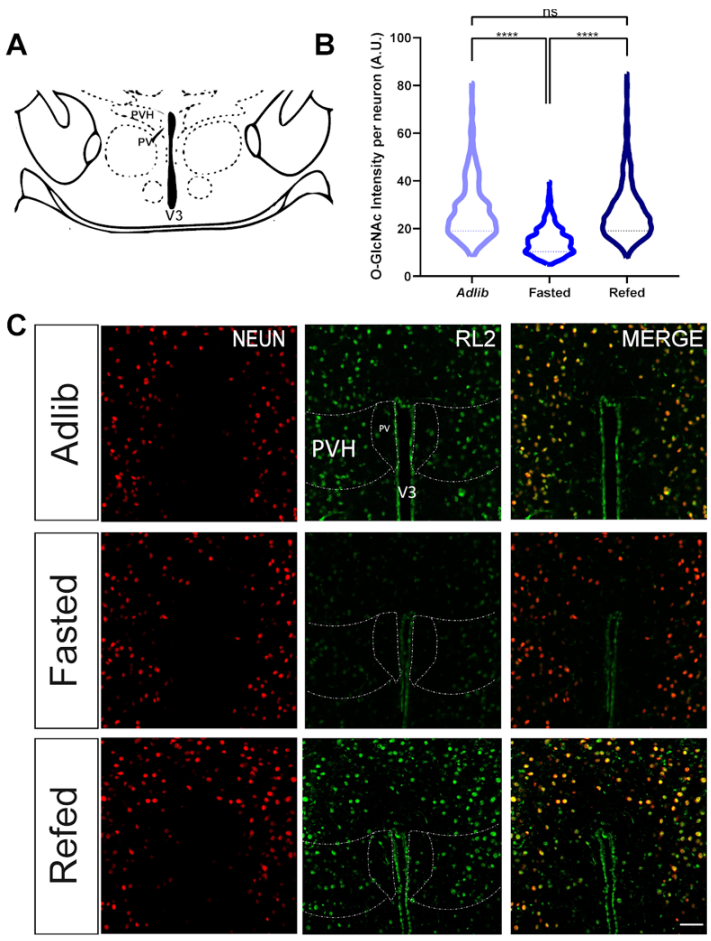

Figure 1.2: Effects of fasting and refeeding on protein O-GlcNAcylation in mouse paraventricular nucleus (PVN, PVA, or PVH) of the hypothalamus, located close to the third-ventricle (V3). (A) Image of mouse brain atlas showing the PVN region (bregma -0.82) [20]. (B-C) O-GlcNAc level is quantified using relative O-GlcNAc and neuron (NeuN) specific antibodies. Decreased O-GlcNAc intensity is detected in fasted mice compared to *adlib* and refed mice. (C) Immunohistochemical staining of total O-GlcNAcylation in the mouse brain PVN region from *Adlib*, Fasted, and Refed mice (Scale bar: 50mm). Total of 200-300 cells counted per mouse/condition (n = 3). Data was analyzed with the Kruskal-Wallis test****p <0.0001.

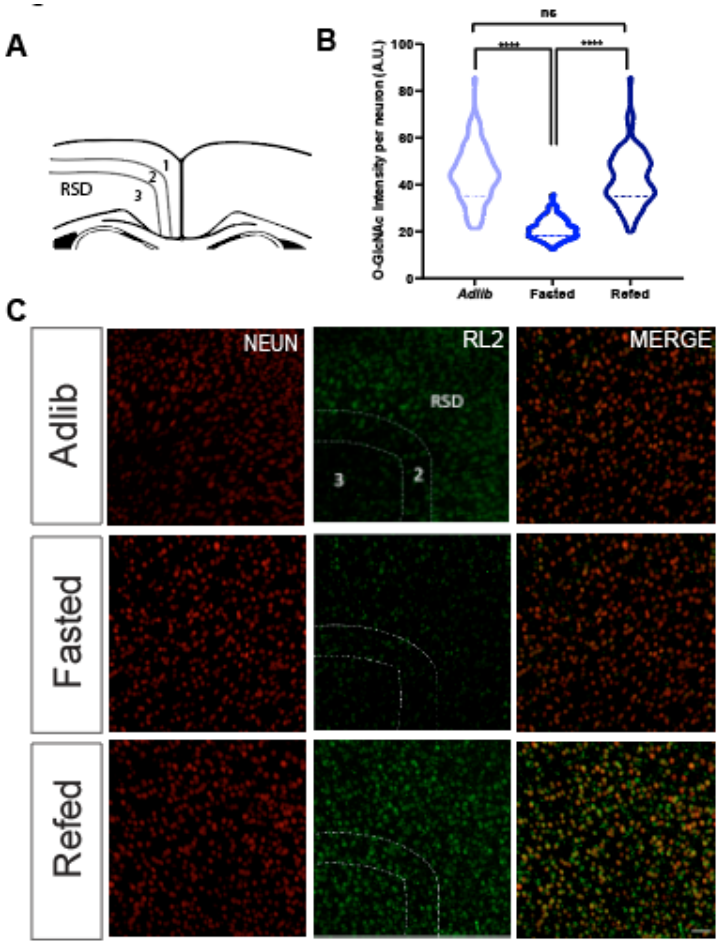

Figure 1.3: Effects of fasting and refeeding on O-GlcNAcylation in the mouse cortex. (A) Image of mouse brain atlas showing the cortex from the brain (Retrosplenial area dorsal (RSD) region, bregma -1.34) [20]. (B-C) Immunohistochemical staining and quantification of total O-GlcNAcylation in the mouse brain RSD region from *Adlib*, Fasted, and Refed mice. O-GlcNAc level is quantified using relative O-GlcNAc and neuron specific (NeuN) antibodies. Decreased O-GlcNAc intensity is detected in fasted mice compared to *adlib* and refed mice (Scale bar: 50mm). Total of 50-100 cells counted per mouse/condition (n=2). Data was analyzed with the Tukey's multiple comparisons test, ****p <0.0001.

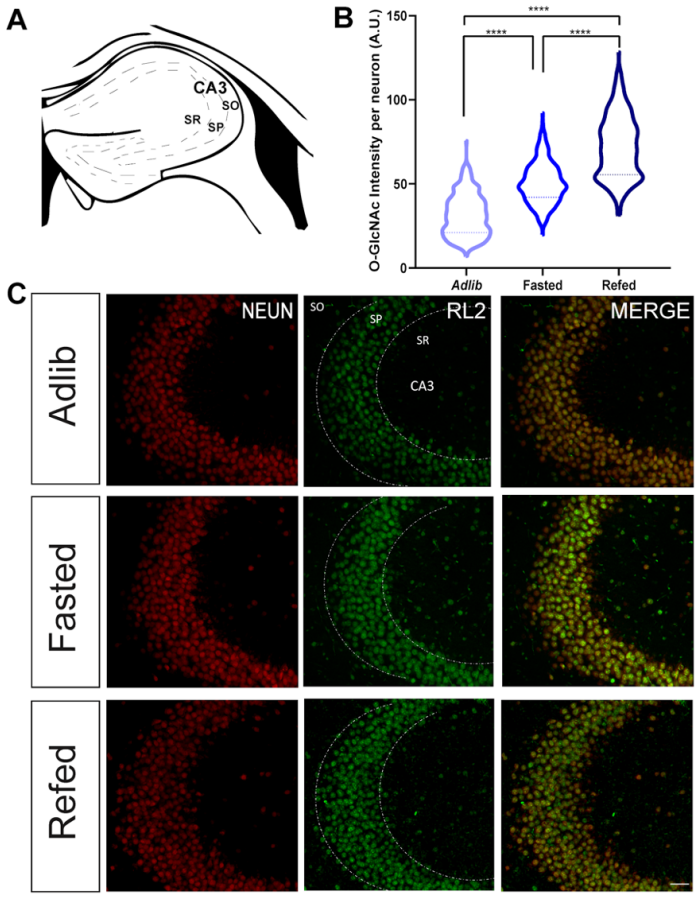

Figure 1.4: Effects of fasting and refeeding on O-GlcNAcylation in the mouse hippocampus CA3 region. (A) Image of mouse brain atlas showing the hippocampus from the brain atlas (bregma -1.34) [15] (B-C) Immunohistochemical staining and quantification of total O-GlcNAcylation in the mouse brain hippocampus CA3 region from *Adlib*, Fasted, and Refed mice. O-GlcNAc level is quantified using relative O-GlcNAc and neuron specific (NeuN) antibodies. Increased O-GlcNAc intensity is detected in fasted mice compared to *adlib* and refed mice (Scale bar: 50mm). Total of 100-200 cells counted per mouse/condition n=2. Data was analyzed with Kruskal-Wallis test, ****p <0.0001, ****p <0.0001, ****p <0.0001.

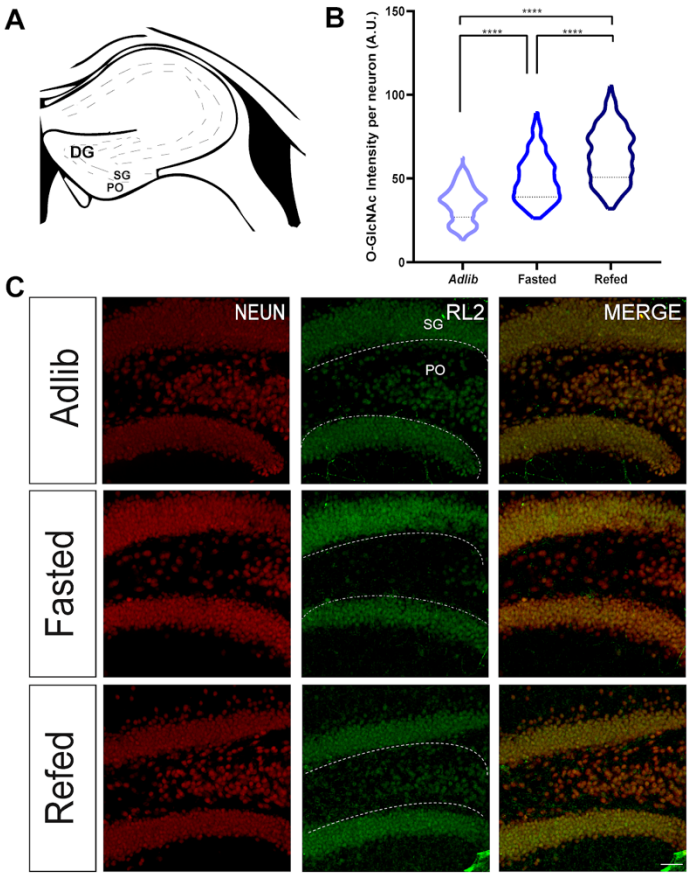

Figure 1.5: Effects of fasting and refeeding on O-GlcNAcylation in the mouse hippocampus DG region. (A) Image of mouse brain atlas showing the hippocampus from the brain atlas (bregma -1.34) [20]. (B-C) Immunohistochemical staining and quantification of total O-GlcNAcylation in the mouse brain hippocampus DG region from *Adlib*, Fasted, and Refed mice. O-GlcNAc level is quantified using relative O-GlcNAc and neuron specific (NeuN) antibodies. Increased O-GlcNAc intensity is detected in fasted mice compared to *adlib* and refed mice (Scale bars: 50mm). Total of 100-200 cells counted per mouse/condition (n=2). Data was analyzed with the Kruskal-Wallis multiple comparisons test,****$p<0.0001$.

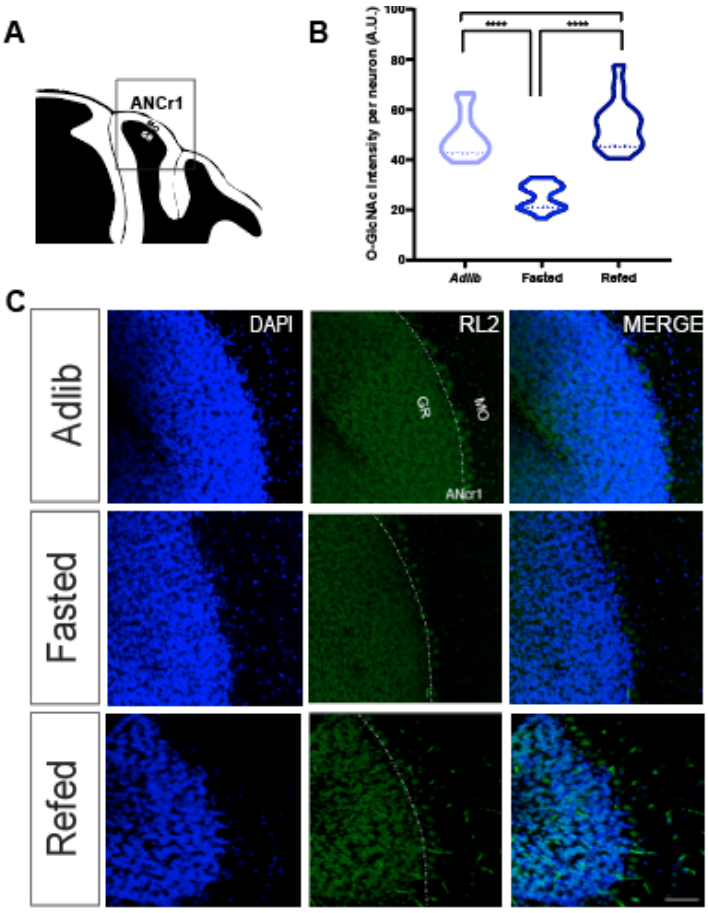

Figure 1.6: Effects of fasting and refeeding on O-GlcNAcylation in the mouse hippocampus Cerebellum region. (A) Image of mouse brain atlas showing the cerebellum ANcr1 region from the brain atlas (bregma -5.52) [20]. (B-C) Immunohistochemical staining and quantification of total O-GlcNAcylation in the mouse brain RSD region from *Adlib*, Fasted, and Refed mice. O-GlcNAc level is quantified using relative O-GlcNAc and DAPI antibodies. Decreased O-GlcNAc intensity is detected in fasted mice compared to *adlib* and refed mice (Scale bar: 50mm) . Total of 15-20 Purkinje cells counted between the molecular and granular layer per mouse/condition (n=1). Data was analyzed with the Tukey's multiple comparisons test. ****p <0.0001.

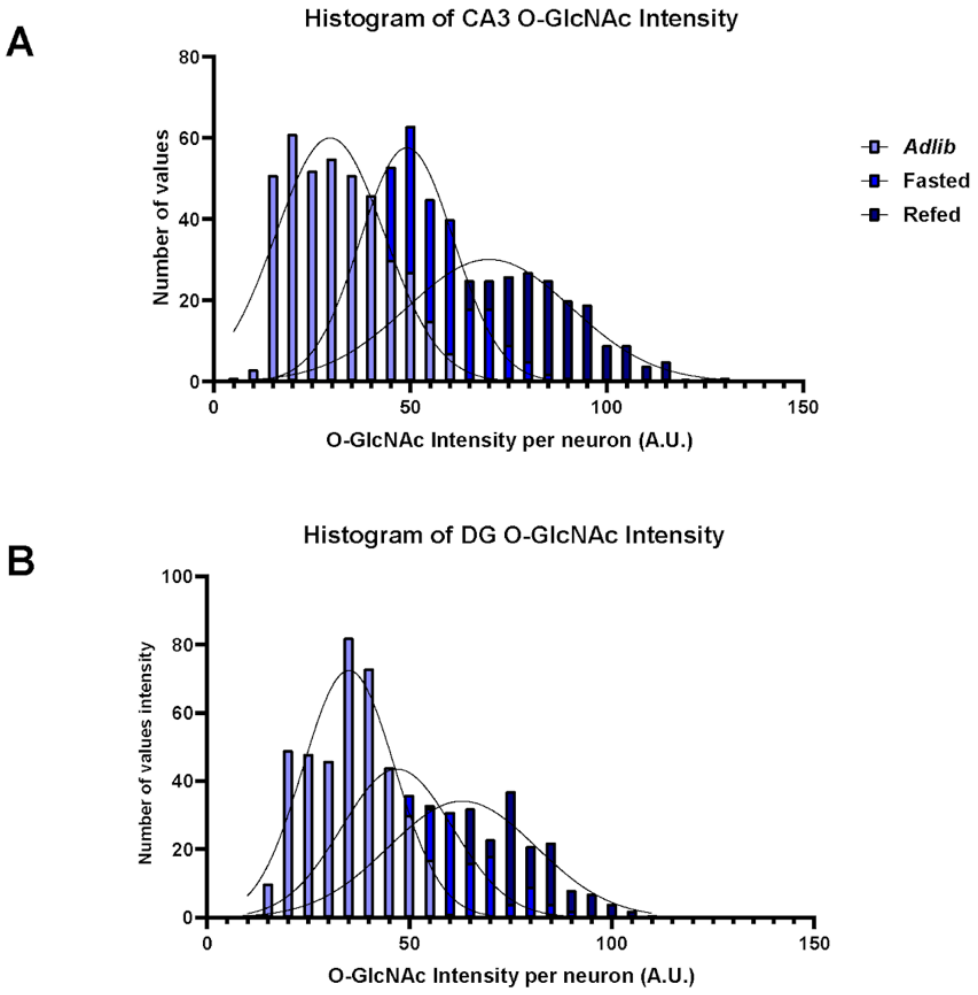

Supplementary Figure 1.1: Histogram of O-GlcNAc intensity profile of DG and CA3 neurons. (A) CA3, and (B) DG O-GlcNAc distribution demonstrating the refed mice have the highest O-GlcNAc values compared to *adlib* and fasted groups.

METHODS

Fasting/Refeeding Studies in Mice

Age-matched (8-weeks old) male C57Bl/6J mice were housed at 22-24°C using a 12h light/12h dark cycle with ad libitum access to standard mouse chow and water. Care of animals and diet change procedures were approved by the BNH vivarium and use Committee. For fasting and refeeding studies, food was removed, and then replaced 24 hours later. All mice were sacrificed and the brain samples were collected in the early afternoon, which eliminated the effect of circadian rhythm in our study. The manipulations in diet and blood glucose measurements were matched to the start of the "lights-on" cycle. Blood was sampled from the tail vein, and glucose levels were measured with a glucometer (Onetouch Ultra 2). Mice were then perfused with 4% PFA, brains were harvested and collected, then the following day brains were sectioned with Compresstome® VF-300 Vibrating Microtome (Tissue Slicer).

IHC- immunohistochemistry fluorescence

Mice were transcardially perfused with cold 4% (wt/vol) paraformaldehyde (PFA) and the brains were fixed overnight in 4% (wt/vol) PFA at 4 °C, followed by three 10 minutes washes with PBS. Sagittal sections (50 μm) were obtained using a Leica VT 1000s and were stored in an PBS solution at −20 °C. Slices were blocked with 5% (vol/vol) goat serum, 0.1% Triton-X 100 in PBS for one hour, washed 3 times (10 minutes) with PBS, and stained with the primary antibody in 1% (vol/vol) goat serum, 0.1% Triton-X 100 in PBS overnight at 4 °C. The secondary (DF:1500) was applied the following day after (1-2hrs) at room temperature. Slices were mounted Southern Biotech DAPI Fluoromount-

G (C0100-20), coded, and imaged with a Zeiss LSM 780 confocal microscope, with the investigator blind to the genotype. Images were collected from slices spaced 50 μm apart through the region of interest. A minimum of 2-3 slices was quantified for each animal, and a minimum of 2-4 animals were evaluated for each *adlib*/fasted/refed state.

Image quantification and statistical analysis

The quantification of O-GlcNAc expression was based upon DAPI and NeuN criteria. This standardized was based on intensity influenced the adlib mouse, and consideration on area to reference was based brain atlas coordinates [20]. Each region, hippocampus, cortex, cerebellum, and PVN were quantified primarily from cell O-GlcNAc intensity, measured through Image J using the freehand selection tool. In all conditions (adlib, fasted, and refed), all analysis were done in similar fashion blinded to conditions. Cell intensity plotted on GraphPad. Then all data sets were analyzed using repeated-measures two-way ANOVA with Kruskal-Wallis test for nonlinear values and Tukey's multiple comparisons for linear values. Quantifications represent mean ± SD.

REFERENCES

[1]Ashrafi G, Ryan TA. Glucose metabolism in nerve terminals. Curr Opin Neurobiol. 2017;45:156–161. doi:10.1016/j.conb.2017.03.007

[2] Bouché C, Serdy S, Kahn CR, Goldfine AB. The cellular fate of glucose and its relevance in type 2 diabetes. Endocr Rev. 2004;25(5):807–830. doi:10.1210/er.2003-0026

[3] Varki A, Cummings RD, Esko JD, et al., eds. Essentials of Glycobiology. 3rd ed. Cold Spring Harbor (NY): Cold Spring Harbor Laboratory Press; 2015.

[4] Zachara N, Akimoto Y, Hart GW. The O-GlcNAc Modification. 2017. In: Varki A, Cummings RD, Esko JD, et al., editors. Essentials of Glycobiology [Internet]. 3rd edition. Cold Spring Harbor (NY): Cold Spring Harbor Laboratory Press; 2015-2017. Chapter 19.

[5] Zachara NE, Hart GW. O-GlcNAc a sensor of cellular state: the role of nucleocytoplasmic glycosylation in modulating cellular function in response to nutrition and stress. Biochim Biophys Acta. 2004;1673(1-2):13–28. doi:10.1016/j.bbagen.2004.03.016

[6] Ruan HB, Singh JP, Li MD, Wu J, Yang X. Cracking the O-GlcNAc code in metabolism. Trends Endocrinol Metab. 2013;24(6):301–309. doi:10.1016/j.tem.2013.02.002

[7] Hebert LF Jr, Daniels MC, Zhou J, et al. Overexpression of glutamine:fructose-6-phosphate amidotransferase in transgenic mice leads to insulin resistance. J Clin Invest. 1996;98(4):930–936. doi:10.1172/JCI118876

[8] Pekkurnaz G, Trinidad JC, Wang X, Kong D, Schwarz TL. Glucose regulates mitochondrial motility via Milton modification by O-GlcNAc transferase. Cell. 2014;158(1):54–68. doi:10.1016/j.cell.2014.06.007

[9] Cai H, Cong WN, Ji S, Rothman S, Maudsley S, Martin B. Metabolic dysfunction in Alzheimer's disease and related neurodegenerative disorders. Curr Alzheimer Res. 2012;9(1):5–17. doi:10.2174/156720512799015064

[10] Yuzwa SA, Shan X, Macauley MS, et al. Increasing O-GlcNAc slows neurodegeneration and stabilizes tau against aggregation. Nat Chem Biol. 2012;8(4):393–399. Published 2012 Feb 26. doi:10.1038/nchembio.797

[11] Kim C, Nam DW, Park SY, et al. O-linked β-N-acetylglucosaminidase inhibitor attenuates β-amyloid plaque and rescues memory impairment. Neurobiol Aging. 2013;34(1):275–285. doi:10.1016/j.neurobiolaging.2012.03.001

[12] Jacobsen KT, Iverfeldt K. O-GlcNAcylation increases non-amyloidogenic processing of the amyloid-β precursor protein (APP). Biochem Biophys Res Commun. 2011;404(3):882–886. doi:10.1016/j.bbrc.2010.12.080

[13] Lehman DM, Fu DJ, Freeman AB, et al. A single nucleotide polymorphism in MGEA5 encoding O-GlcNAc-selective N-acetyl-beta-D glucosaminidase is associated with type 2 diabetes in Mexican Americans. Diabetes. 2005;54(4):1214–1221. doi:10.2337/diabetes.54.4.1214

[14] Li X, Lu F, Wang JZ, Gong CX. Concurrent alterations of O-GlcNAcylation and phosphorylation of tau in mouse brains during fasting. Eur J Neurosci. 2006;23(8):2078–2086. doi:10.1111/j.1460-9568.2006.04735.x

[15] Lagerlöf O, Slocomb JE, Hong I, et al. The nutrient sensor OGT in PVN neurons regulates feeding. Science. 2016;351(6279):1293-1296. doi:10.1126/science.aad5494

[16] Howarth C, Gleeson P, Attwell D. Updated energy budgets for neural computation in the neocortex and cerebellum. J Cereb Blood Flow Metab. 2012;32(7):1222–1232. doi:10.1038/jcbfm.2012.35

[17]Li X, Lu F, Wang JZ, Gong CX. Concurrent alterations of O-GlcNAcylation and phosphorylation of tau in mouse brains during fasting. Eur J Neurosci. 2006;23(8):2078–2086. doi:10.1111/j.1460-9568.2006.04735.x

[18] Silver IA, Erecińska M. Extracellular glucose concentration in mammalian brain: continuous monitoring of changes during increased neuronal activity and upon limitation in oxygen supply in normo-, hypo-, and hyperglycemic animals. J Neurosci. 1994;14(8):5068–5076. doi:10.1523/JNEUROSCI.14-08-05068.1994

[19] Ruan HB, Dietrich MO, Liu ZW, et al. O-GlcNAc transferase enables AgRP neurons to suppress browning of white fat. Cell. 2014;159(2):306–317. doi:10.1016/j.cell.2014.09.010

[20] Lein ES, Hawrylycz MJ, Ao N, et al. Genome-wide atlas of gene expression in the adult mouse brain. Nature. 2007;445(7124):168–176. doi:10.1038/nature05453

CHAPTER 2

O-GlcNAcylation is necessary for PV neuronal health and survival

Parvalbumin (PV) neurons are a subclass of inhibitory interneurons that are fast-spiking with high energy demands. The PV neurons are essential for the formation of functional neuronal circuitry and the maintenance of excitatory/inhibitory (E/I) balance in the brain. The role post-translational modifications (PTMs) such as phosphorylation and ubiquitination in regulation of PV neuron function have been well characterized. However, the implication of O-GlcNAcylation, a metabolism-sensitive PTM which acts on serine/threonine residues, in these types of neurons remains unknown. To uncover the role of metabolic sensing via O-GlcNAcylation, we have generated a PV neuron-specific O- GlcNAc transferase knockout (PV.OGT-KO) mouse. Our results show that loss of O-GlcNAc signaling induces a distinctive loss of viability of PV neurons in different brain regions; cerebellar neurons are more vulnerable than neurons in cortex and hippocampus. Specifically, Purkinje neurons were significantly affected due to their enrichment in O-GlcNAcylation under normal conditions, which resulted in reduced cerebellar cytoarchitecture, motor impairments, and lower survival rate of PV.OGT-KO mice. These results likely indicate that O-GlcNAcylation regulates molecular pathways that are important for PV neuron survival.

INTRODUCTION

Neurons are anatomically and metabolically diverse cells with high energy demand [1,2]. Parvalbumin- GABAergic-inhibitory (PV) interneurons rely heavily on glucose as the main energy source. Considering the fact that single action potential uses roughly 10 million ATP, firing at 300-400 Hz requires precise metabolic regulation for the maintenance of energy homeostasis [3, 4]. PV neuron function is regulated viaPTM such as phosphorylation, ubiquitination, and palmitoylation [4]. However, little is known about the role of O-GlcNAcylation, a PTM, on PV neuron development, survival and function. We hypothesized metabolic sensing via OGT and O-GlcNAcylation is essential for PV neurons to maintain energy homeostasis. Here, we investigated the role of OGT and O-GlcNAcylation in PV neurons by generating PV-specific OGT knock-out mice *in vivo*. OGT regulates O-GlcNAcylation of over 4,000 cytoplasmic, nuclear and mitochondrial proteins and plays critical roles in both neuronal health and survival [5-7]. It has been well established that *ogt* gene deletion can cause early neonatal embryonic lethality because of the role its essential function cell-cycle and proliferation [5]. Therefore, conditional gene targeting approaches are used to study the role OGT in different tissues *in vivo*, including the brain [6]. OGT is encoded on the X-chromosome [5]. Creation of the OGT mice requires LoxP restriction sites on both sides of exon 1 (206-232 amino acid) [5]. Previous studies demonstrated that the loss of OGT in forebrain excitatory neurons leads to neurodegeneration [6]. However, acute deletion of OGT (by crossing OGT floxed mice with αCaMKII-CreER^{T2}) using a more tamoxifen-induced Cre- specifically perturbs the function of excitatory neurons in hypothalamus [7]. Using this model, the authors have demonstrated that the removal of OGT can cause

hyperphagia and obesity because KO mice couldn't stop eating [7]. Both of the studies above used similar mouse models calcium/calmodulin-dependent protein kinase II alpha (αCaMKII-cre) crossed with OGT floxed mice, however, they have achieved different sets of phenotypes [6,7]. One phenotype showed neurodegeneration [6] while the other study showed feeding circulatory impairments and obesity upon deletion of OGT [7]. In glia, studies have shown the loss of OGT (P_0-$Cre^{-/+}$, $OGT^{loxP/lox}$) induces demyelination of neurons, motor dysfunction by inducing muscle weakness, gait abnormalities, and sensory nerve impairment [8,9]. This study aimed to develop new strategies to study peripheral neuropathy as it is caused by altered metabolic functions of axonal support and myelination. In sensory neurons, OGT knockout (*Nav1.8-Cre*$^{-/+}$ $Ogt^{loxP/Y}$) directly caused striking hyposensitivity to mechanical and thermal stimulation [10]. In sensory neurons, the deletion of OGT whether during development or in adults has been shown to be associated with neuronal cell loss, and confirming OGT's essential role for sensory neuron survival [10].

OGT is preferentially localized at pre- and post-synaptic sites and involved in axonal branching and development [11,12]. Furthermore, total O-GlcNAcylation is higher during prenatal development and it decreases with age [13]. Each neuron relies on OGT differently, most of the studies highlighted earlier have shown OGT as a metabolic sensor, myelination activator, and is necessary for excitatory neuronal health and survival [6-10].

O-GlcNAcylation plays a fundamental role in regulating cell division, differentiation, transcription and apoptosis [14]. Both the loss or the gain of O-GlcNAcylation may have neuroprotective or neurodegenerative functions. The loss

of OGT has been explored in excitatory neurons, Schwann cells, sensory neurons and specifically in AgRP neurons [6-10]. Mechanisms regulating tight control of neuron-type specific O-GlcNAcylation levels remains an outstanding question.

Here, we studied the role of O-GlcNAcylation in PV neuronal health and survival. To specifically knock-out OGT in PV neurons, we crossed PV-Cre with OGT-floxed mice. It is important to note that the first generation of female mice are heterozygous due to X-inactivation and males have only one OGT allele. Thus, only male mice are used in our OGT knock-out experiments. Our goals were to determine (1) Validate O-GlcNAcylation status in PV.OGT KO mice, (2) identify *how* OGT loss affect PV neuron survival rate in different brain regions, (3) and different age groups, and (4) assess behavioral characteristics of PV.OGT KO mice. We have found that loss of OGT in PV neurons cause reduction in PV neuron number in the cerebellum, specifically Purkinje neurons, as early as 2-weeks of age. Overall, PV.OGT KO mice don't survive past 3-months of age, have reduced weight gain, and motor impairment. In sum, our data suggest that OGT is necessary for PV neuronal health and survival.

RESULTS

Generation of PV-specific OGT knock-out mice

We generated a knocked-out transgenic of PV.OGT KO mice by crossing the floxed *ogt* (OGT fl) mouse with a PV-CRE transgenic mouse (Fig. 1A). Cre-expression in PV neurons turns on postnatally in the cortex, hippocampus, thalamus, and hypothalamus [15] (SFig. 4A). However, the cerebellum cre-recommendations turn on embryonic day 15.5 [16](SFig. 4A). Mice were produced at normal frequencies, however, PV.OGT KO mice display reduced brain size/weight at P30 and have smaller cerebellum at P30 and P90 (Fig. 1B,1C). PV.OGT KO (***Pvalb***$^{(cre)Arbr}$ x **Ogt**$^{flox/y}$) mice have hindlimb clasping at P16 and start to show severe tremor as well as minor trunk curvature at P30. Furthermore, KO mice began to show significant weight loss at 3-weeks of age (Fig. 2A). Due to severe food/water intake reduction at P30 (Fig. 2B, 2C), motor defects and paralysis by P90, PV. OGT KO mice don't survive past 3-months of age (Fig. 1D).

Decrease in overall weight gain in PV-OGT KO mice

To ascertain whether a decrease in body weight exhibited by PV.OGT KO mice can be ascribed to a decrease in adipose mass or to other contributors such as lean muscle and water mass. We performed an Echo MRI to measure total fat mass, lean mass, and free water mass (Fig. 3). There was a greater difference in adipose and muscle tissue mass (Fig. 3A and 3C) compared to water (Fig. 3B). When it comes to assessing between different ages of KO mice (1-month and 3-month), the older KO mice display a significant amount of fat reduction (Fig. 3D) compared to WT mice. Suggesting 3-months KO mice overall weight gain flat out after 1- month of age and they don't gain fat mass

but instead gain muscle and water mass compared to 1-month KO mice (Fig. 3B, 3C). To measure muscle strength, coordination and balance, a hanging wire and grip test were performed. The grip test showed a significant difference between the WT and KO groups, KO mice muscle strength are weaker (Fig. 4A and 4B). Latency to fall in the hanging wire test was significantly shorter in KO mice than in WT mice (Fig. 4C). Despite this, we concluded we see a difference in muscle morphology from the muscle extraction images from P30 WT and KO groups (Sfig. 2C). However, further histology analysis is needed to confirm this finding. Finally, we do note that muscle tissue has PV-RNA expression (SFig. 4B) and Cre levels turn on ~P48 (SFig. 4A). Perhaps, this may predict morphological abnormalities in the muscle. All together, these results suggest that the deletion OGT in PV neurons caused impairment in motor functions and muscle strength.

Behavioral panel characterization of KO mice shows high levels of anxiety and motor defects

The PV.OGT KO mice exhibited abnormalities in a neurological screen which includes right/left reflex, home cage behaviors, motor, muscular abilities, paw clasping, and empty cage behaviors (Fig 5). Importantly, hundred percent of KO mice both 1-month and 3- months of age displayed unusual body and limb tone, and reactivity of stereotypies (Fig. 5A). Notability, 3-months (older) KO mice have 75% trunk curl behavior and righting reflex (Fig. 5A). To test for fine motor dexterity, emotional state, and cognition with little stress imposed on mice, they were subjected to nest-building observation. The PV.OGT KO mice show a significant decrease in the nest building and

display disorganized usage of the nestling material compared to the WT mice (Fig. 5B). The open field test was performed to evaluate reaction to novelty, locomotor and anxiety-like behaviors (Fig. 6). The distance traveled and velocity are significantly decreased in PV.OGT KO mice in both ages compared to WT (Fig. 6B, 6C). However, the travel paths and time spent in the center zone were increased in PV.OGT KO mice (Fig. 6C), as seen the path traveled (Fig. 6A) older KO mice rarely move from the center. Here we investigated the effect of genetic deletion of OGT on auditory fear conditioning, during which we paired a foot shock stimulus (unconditional stimulus), which elicits the naturalistic behavior of freezing (defined as absence of all movement except breathing), with a tone (conditioned stimulus), which does not elicit freezing on its own (SFig. 1A). After 5 such pairings, the tone is thought to become associated with and predict and shock, and can elicit learned freezing, which indicates fear. We found an overall significant difference in reduced freezing behavior in KO, reduced in freezing both on contextual conditioning after cued conditioning/habituation (SFig. 1B and 1C). In summary, the behavioral assessment showed mice lacking the OGT gene in PV neurons have higher levels of anxiety like behaviors, locomotor defects, muscle abnormalities, and hippocampus-dependent and -independent learning processes are impaired.

OGT knock-out validations

We have examined OGT activity dependent O-GlcNAcylation level in brain tissue collected from WT and PV OGT KO mice. By staining with PV and O-GlcNAc-specific antibodies, we compare their respective levels in WT vs PV.OGT KO mice. To quantify O-GlcNAcylation level, we compare the O-GlcNAc fluorescent intensities in

PV neurons between a KO and WT mouse (Fig. 7). Our analysis revealed a total of 50% O-GlcNAc signal in KO mice compared to WT at P30 (Fig. 7D and 7E). Thus, in PV-specific OGT knockout mice brain, a large majority of PV neurons have lost their O-GlcNAcylation. In addition, we have analyzed non-PV neurons/glia in the cortex and CA1 region of the hippocampus to confirm specificity of KO and observed no changes in the O-GlcNAc levels (SFig. 5A and 5B).

OGT deficiency in PV neurons caused impaired survival in the cerebellum

One of the first brain regions we analyzed was the cerebellum, due to smaller cerebellar morphology at P30 in PV.OGT KO mice (Fig. 1B) and motor impairment. The loss of purkinje cells was confirmed by immunostaining with PV and calbindin (Fig. 8B and 8C). In addition, we found a disorganization of PV neurons and loss neuronal processes in the KO mice (Fig. 8D). We then quantified purkinje cell number both at molecular and granula layers (Fig. 9, SFig. 3). Deletion of OGT altered normal cerebellar organization, reduced purkinje cell number (Fig. 9A-C). In addition, as PV.OGT KO mice age, we found further reduction of Purkinje cell number and size at P30 (Fig. 9D-F) concomitant with loss of motor coordination. The loss of Purkinje cells is correlated with a significant decrease in width of molecular and not granular layer at P30 in the cerebellum of PV.OGT KO mice and no significant finding at P16 in KO mice was observed (SFig. 3A-B).

Loss of O-GlcNAcylation in PV.OGT KO mice leads to PV neuronal degradation in hippocampus and cortex

PV neuron loss was also observed in the hippocampus via immunostaining of PV (Fig. 10A-C) at P16 and P30. PV positive cells were counted from CA1-DG from KO and WT mice. The PV neurons loss in CA1 and CA3 was observed at P16 in KO mice (Fig. 10D). The cerebellum shrinkage and motor defects observed in KO mice led us to analyze the motor cortex next. At the motor cortex, we detected age-dependent reduction in PV neuron counts (Fig. 11A-E).

DISCUSSION

O-GlcNAcylation is a metabolism-sensitive and highly dynamic post-translational modification [17]. A growing number of studies examined the effect of conditional and non-conditional deletion of OGT, many have found neuronal loss [7,18]. In this study, we generated PV neuron specific OGT knockout mice to investigate OGT's role in PV neurons. We found that loss of OGT in PV neurons results in postnatal lethality at 3 months of age with severe age-dependent neurological defects. We also demonstrated that loss of OGT in PV neurons does perhaps affect the global development behavior of mice since we observed loss of Purkinje cells early on at P16. The phenotypes of motor defects, muscle weaknesses, and PV neuronal loss may be solely due to neuronal migration and developmental defects.

The functional role of O-GlcNAcylation is only determined for limited number of proteins [9,19]. Many of the known O-GlcNAcylated proteins are involved in cytoskeletal organization, synaptic function, transcription and organelle trafficking. It is difficult to pin-point the exact molecular mechanism of PV-loss phenotype without performing detailed O-GlcNAcome analysis. For example, mitochondrial dysfunction may lead to axonal degeneration which initiates cell death and neuronal loss [20]. Notably, glucose levels and OGT can affect mitochondrial motility and transport [21]. Thus, perhaps our KO mice have metabolic changes in their glucose regulation and shuttle into the HBP which can ultimately affect OGT activity on proteins. Overall, it is likely that the observed phenotypes are generated by multiple pathways affecting PV neuron health and survival.

Using mice lacking OGT in PV neurons, we have examined and shown that Purkinje cells are more vulnerable to changes to O-GlcNAcylation than compared to the

other PV positive neurons in cortex and hippocampus (Fig.8, Fig. 10 and Fig. 11). Cre-recombination turns on embryonically in the cerebellum [15,16], suggesting why we see more PV cell disorganization and loss in the cerebellum at P16 and P30 (Fig. 8B and 9A). Overall, the -Cre expression at E15.5-E19 can affect Purkinje cell migration, docking, and synapse formation.

Previous studies have suggested that OGT and O-GlcNAc-modified proteins are highly enriched in the Purkinje cells and nerve terminals compared to excitatory neurons [22]. Excitatory and inhibitory neuronal inputs are quite important for motor coordination, and Purkinje cells are the sole output for the cerebellar cortex. The motor impairment present in the OGT knock-out mice (Fig.4 and Fig 6), which may be due to purkinje cell death at early ages in post-development (Fig. 9B and 9E).

O-GlcNAcylation seems to play a complex role in PV neurons at different development stages. We have shown that it plays a neuroprotective role at later stages. The loss of OGT can lead to miswiring of neuron circuitry and excitatory/inhibitory imbalance. It is noteworthy to point out that loss of OGT in inhibitory-neurons have more severe phenotype than excitatory neurons. Perhaps, this is due to higher energy demands and overall consumption of glucose and required OGT activity for metabolic sensing. Further analysis of mechanism regulating OGT activity in PV neuron development, health and survival is necessary to fully PV neuronal pathways. In the future, we plan to preform O-GclNAcome of PV neurons to evaluate proteins effect by O-GlcNAcyaltion and use cre-tamoxifen induced model to differentiate between developmental vs degenerative phenotypes.

FIGURES

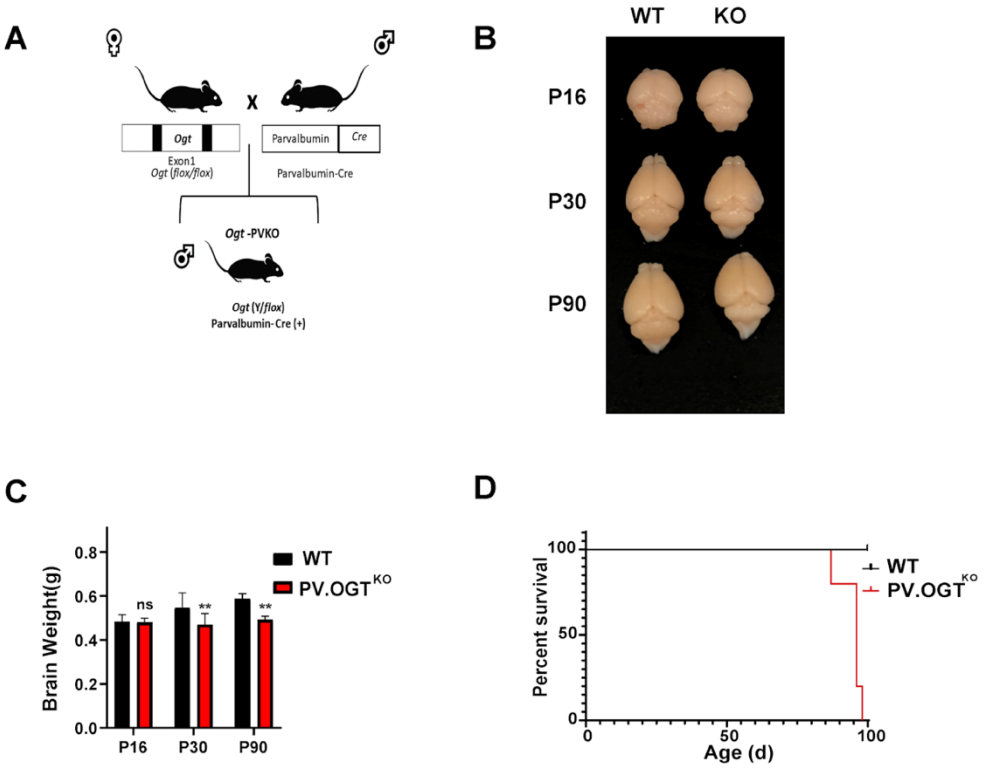

Figure 2.1: PV.OGT-KO mice brain size is reduced compared to WT (A) Genetic cross scheme. (B) Brain tissue collected from P16-P90 mice. (C) Brain tissue weights in male P16 WT (n = 6) and PV.OGT KO (n = 7), P30 WT (n=5) and PV.OGT KO (n = 8), P90 WT (n=5) and PV.OGT KO (n=5). Two-Way ANOVA Sidak's multiple comparisons test, **p= 0.00427, **p=0.0021. (D) PV.OGTKO mice don't survive past 3 months of age.

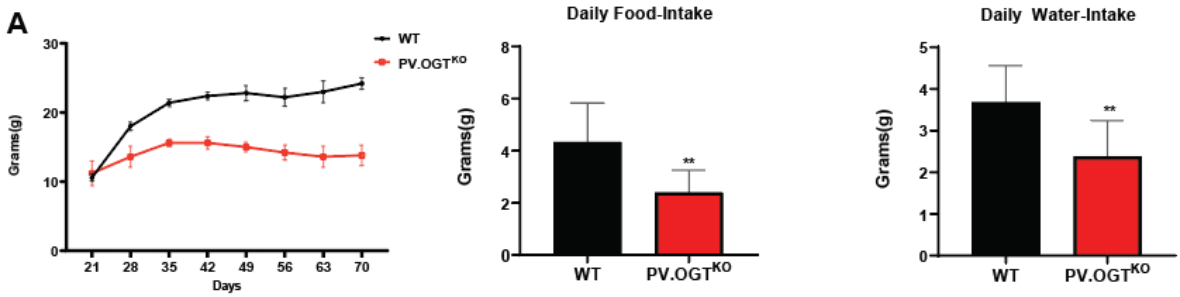

Figure 2.2: OGT phenotypic characterization (A) PV.OGTKO mice display significantly reduced weight gain beginning at 4- weeks of age. (B, C) Decreased food and water intake in PV.OGTKO mice. WT (n=8) and KO (n=8). Grams weight per animal for 10 days (B) food-intake unpaired t-test, **p= 0.0024; water- intake (C) unpaired t-test, **p= 0.0027.

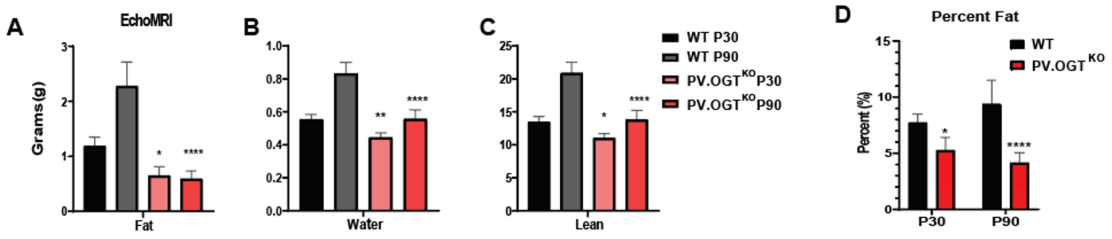

Figure 2.3: The body composition analysis (with EchoMRI) WT and KO mice. (A-C) Weight comparison in fat, water and muscle at P30 and P90. (D) Percent fat comparison WT and KO. WT P30 (n=5), WT P90 (n=4), KO P30(n=6), KO P90 (n=4). Data is analyzed using Tukey's multiple comparisons tests. *p< .01, **p<.005, ****p<0.0001.

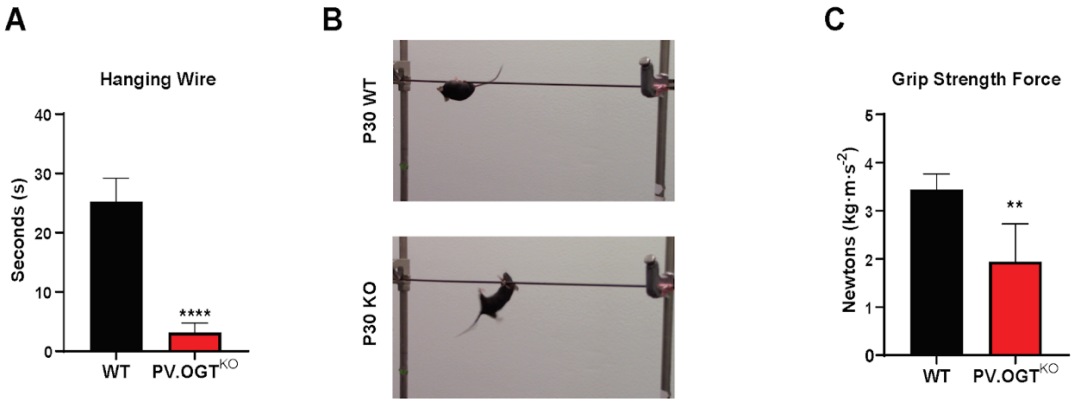

Figure 2.4: Behavioral assessment of muscle weakness in PV.OGTKO mouse. (A) Grip strength force of P30 WT vs. PV.OGT KO. Forelimb grip strength was significantly greater in the WT mice compared to the PV.OGT KO mice. WT (n=5) and KO (n=6). Unpaired t-test, **p= 0.0034. (B) Image showing PV.OGT KO mice falling from hanging wire in less than 2 seconds. (C) Hanging wire test (P30) WT vs. PV. OGT KO. For the hanging wire test, the survival proportion of the WT mice was significantly greater than that of the PV.OGT KO mice. WT (n=5) and PV.OGT KO (n=6). Unpaired t-test, ****p <0.0001.

A

	WT		PV-OGT	
	n=5	n=4	n=6	n=4
General Health	Younger	Older	Younger	Older
Unusual body tone	0.00%	0.00%	100.00%	100.00%
Unusual limb tone	0.00%	0.00%	100.00%	100.00%
Home cage behaviors				
Solitary sleeping	0.00%	0.00%	0%	25%
Motoric, muscular abilities				
Trunk curl	0.00%	0.00%	0.00%	100.00%
Righting reflex	100.00%	100.00%	100.00%	75.00%
Forepaw Reaching	100.00%	100.00%	100.00%	0.00%
Postural Reflex	80.00%	100.00%	50.00%	0.00%
Ref lexes				
Eye blink	0.00%	0%	16.67%	0.00%
Ear twitch	40.00%	100%	33.33%	0.00%
Whisker response	40.00%	75%	16.67%	0.00%
Whisker Whisking	80.00%	100%	0.00%	0.00%
Reactivity				
Moving away on petting	100.00%	100.00%	50.00%	0.00%
Struggling on restraint	100.00%	100.00%	100.00%	50.00%
Vocalizing on restraint	100.00%	50.00%	16.67%	0.00%
Dowel biting (3 pt. scale)	1.40	1.00	1.50	0.00
Stereotypies	0.00%	0.00%	100.00%	100.00%
Cage exploration (3 pt. scale)	3.00	3.00	1.33	0.25

B

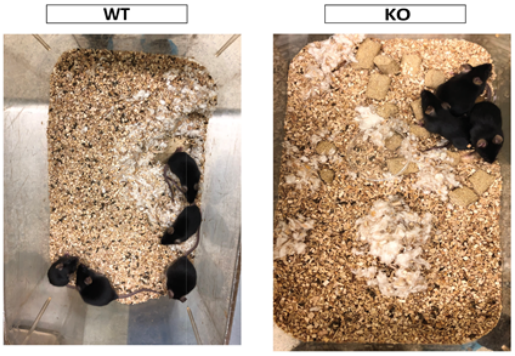

Figure 2.5: Neuroscreen assessment of young and old WT and PV.OGT KO animals. (A)The table shows a general health screen of mice. 3-months PV.OGT KO mice display Trunk curl, muscle abilities, righting reflex, and higher stereotypies behavior compared to younger PV.OGT KO and WT littermates. (B) Representative images of nest building. Images show nest building after 24 h following the introduction of nestling in among all experimental groups.

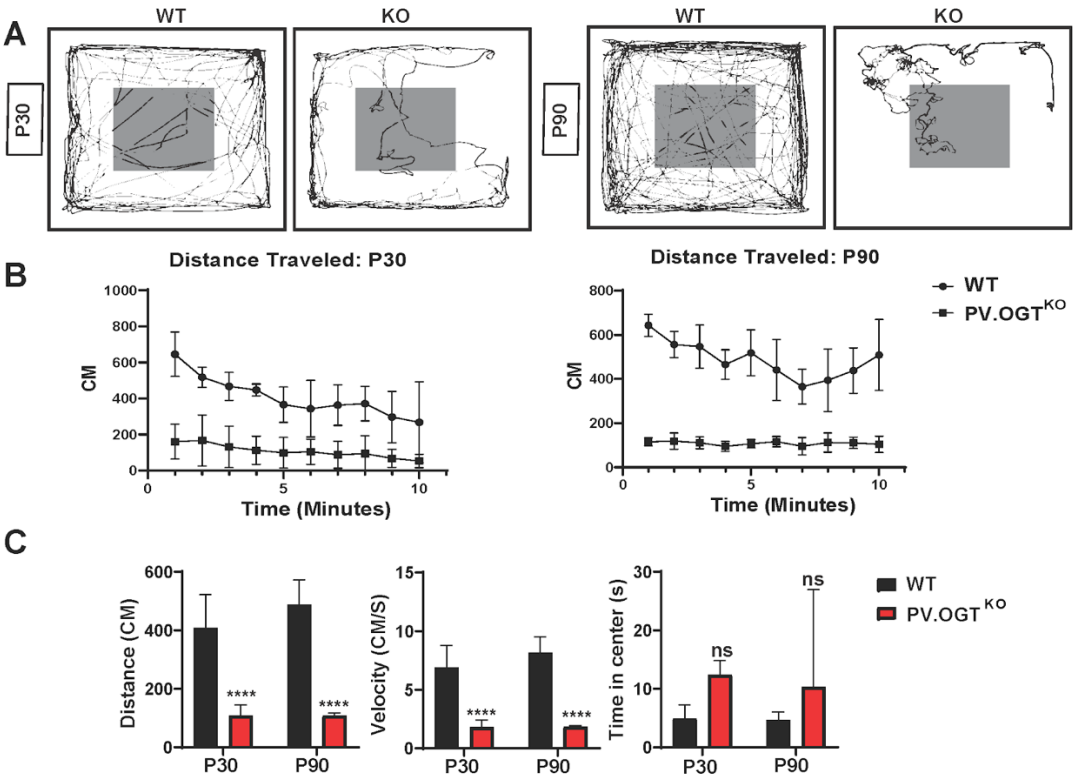

Figure 2.6: Motor impairments in PV.OGT KO as early as P30 (A) In an open field test, PV.OGT KO mice showed promoting behavior to spend more time in the middle of the quadrant of the box and in total distance traveled. (B) Overall, deficits in distance traveled in P30 and P90 KO mice. (C) Reduction in velocity, distance traveled, and increased in time spent in the center. WT P30 (n=5), WT P90 (n=4), KO P30 (n=6), KO P90 (n=4).Data was analyzed by Sidak's multiple comparisons test ****p <0.0001.

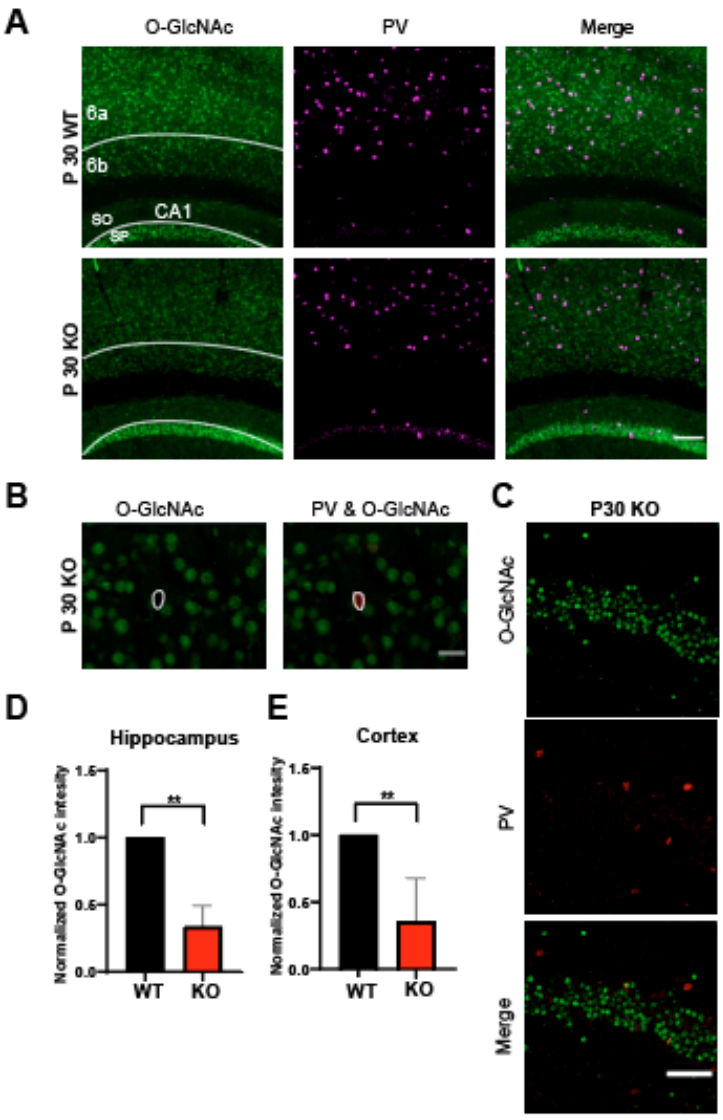

Figure 2.7: Reduction of O-GlcNAcylation in PV neurons positive neurons at P30 in the CA1 and Cortex (somatosensory). (A) Immunostaining of O-GlcNAc (green) and PV (magenta) of KO and WT at P30 (Scale bar:100mm). (B) PV neuron with no O-GlcNAc staining in the cortex of KO mice at P30 (Scale bare: 30mm). (C) Few PV (red) neurons in CA1 are O-GlcNAcylated. (Scale bar: 50mm). (D)Hippocampus region CA1, PV neuron O-GlcNAcylation is reduced in KO at P30 by 50% compared to WT. Total of 5-10 cells were counted per animal (n=2). (E) Similar reduction in O-GlcNAcylation pattern in the cortex of KO mice was observed. Total of 40-50 cells were counted per animal (n=2). Data was analyzed with unpaired t-test and normalized to WT intensity. **p<.007

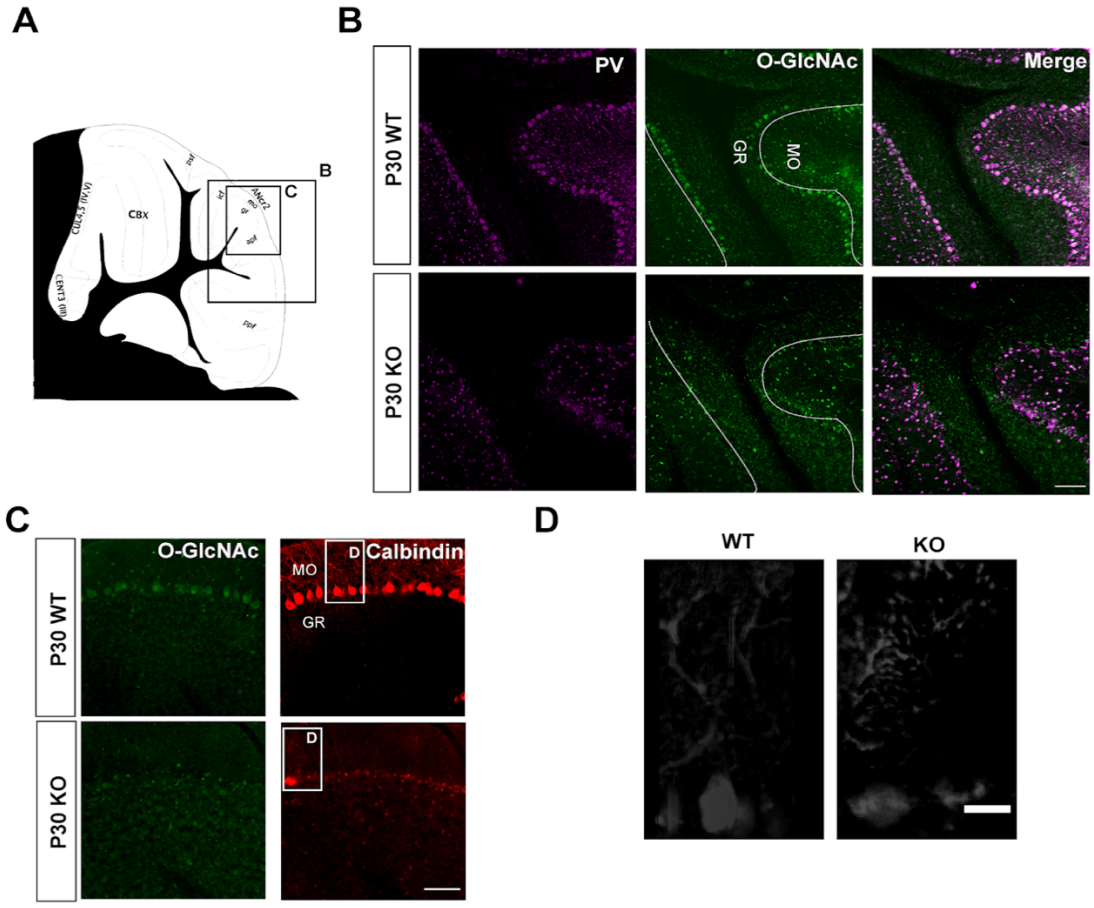

Figure 2.8: Loss of PV neurons, especially, purkinje cells at P30 of age in KO mice (A) Brain atlas image of the cerebellum showing all lobs with highlighted boxes for figures B and C.(Scale bar: 50 mm) (B) PV (magenta) and Rl2 (green) staining of cerebellum highlighting PV neuron loss and disorganization. (C) Complete loss of axons and dendrites in KO mice at P30 in positive purkinje cells. Calbindin staining (red) purkinje cells in the ANcr2 region of the cerebellum. The boxes indicated are for figure D. (Scale bar: 100 mm). (D) Degradation of purkinje cell with loss of axon and dendrites compared to WT (Scale bar: 30 mm).

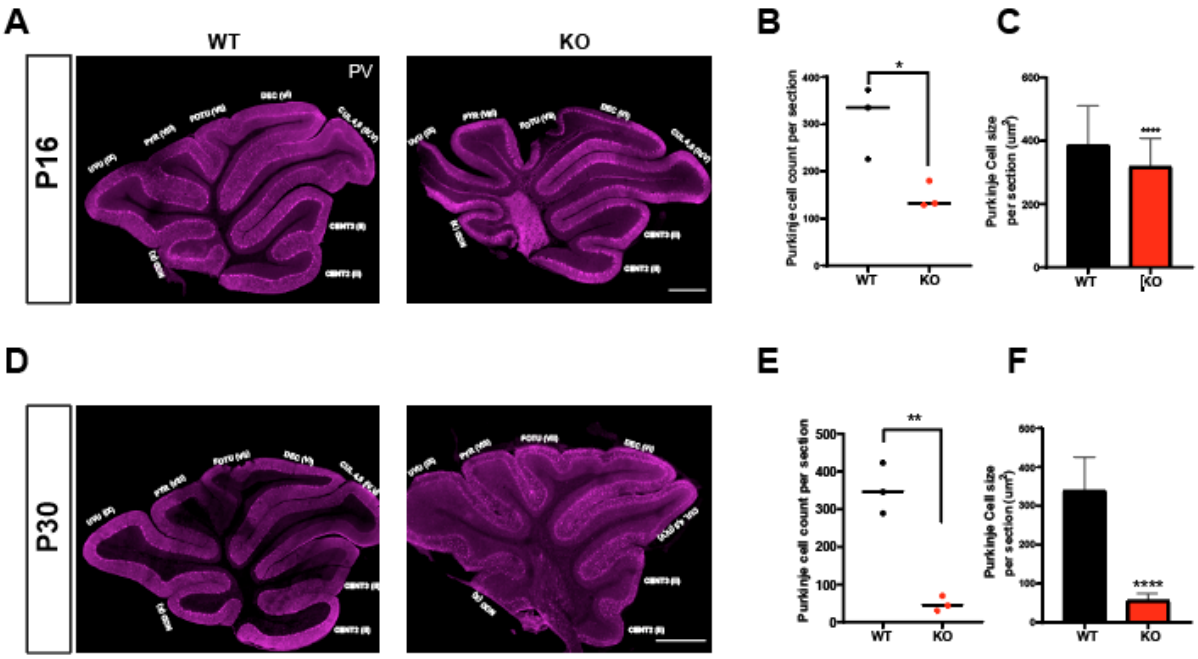

Figure 2.9: Degeneration of Purkinje cells and cerebellar atrophy in PV.OGT KO mice. (A) PV- immunohistochemical staining (magenta) to show gross morphology, minor loss of purkinje cells of brains from P16 WT and KO mice. PV neurons are uniformly disorganized in the cerebellum and disarrayed in the cerebellum of KO mice (Scale bar: 500mm). (B) Purkinje cell counts are reduced in KO mice. (C) Quantification of size of PV-positive Purkinje cells in the cerebellum. Reductions in Purkinje cell size in KO mice at P16. (D) PV- immunohistochemical staining (magenta) to show gross morphology, minor loss of purkinje cells of brains from P 30 WT and KO mice (Scale bar: 500mm). (E)Significantly higher reduction of Purkinje cells counts by P30 compared to P16. (F) Quantification of size of PV-positive Purkinje cells in the cerebellum. Reductions in Purkinje cell size in KO mice at P30. Three sections were analyzed per animal and genotype (n=1). Data analyzed was using unpaired t-test. *p 0.0249, **p 0.0017, **** p<0.0001.

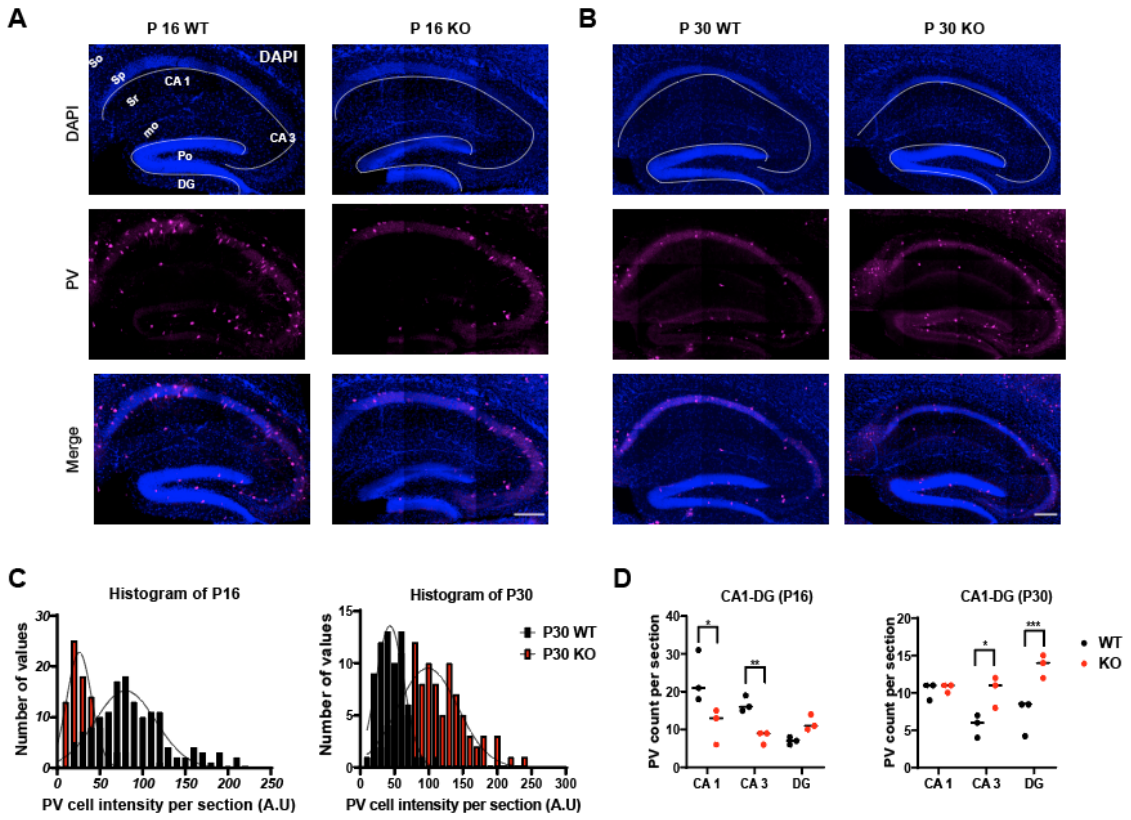

Figure 2.10: Immunostaining of PV staining for hippocampus at P16 and P30. (A) No morphological changes in hippocampus layers and P16. (B) More PV neurons in knockout at CA3 and DG are present in KO compared to WT at P30 (Scale bar: 100 mm). (C)Intensity changes in PV expression are reduced at P16 in KO and increased at P30. (D) PV counts of CA1-DG, P16 KO have more neurons in CA1 and CA3. As KO mice age, they tend to have more neurons in DG and CA3. This perhaps is a failure for proper migration at earlier ages. At least 30-60 cells were counted per section for a total of three sections/per animal (n=1). Data was analyzed with two-way ANOVA -Sidak's multiple comparisons test. *p<.02, **p<.005, ***p<.0006.

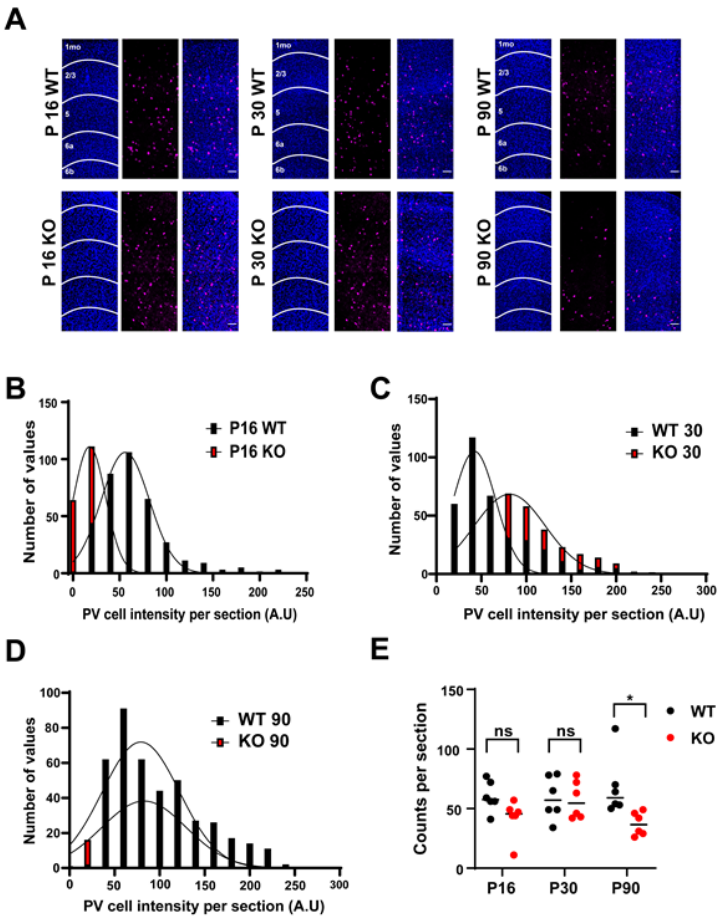

Figure 2.11: Immunostaining images of motor cortex display with aging loss of PV neurons in KO mice. (A) Panel of motor cortex images of WT and KO from P16-P90. Only at P90 PV neuron counts are decreased in KO mice (Scale bar; 50 mm). (B-D) histogram distributions of PV intensity measurements. No significant findings. Only minor shifts in intensity at P16 and P30. (D) PV cell counts were not significant at P16 and P30, however, at P90 in knockouts are reduced. At least 60-100 cells were counted per section for a total of three sections/per animal (n=2). Data was analyzed with two-way ANOVA -Sidak's multiple comparisons test. *p<0.01.

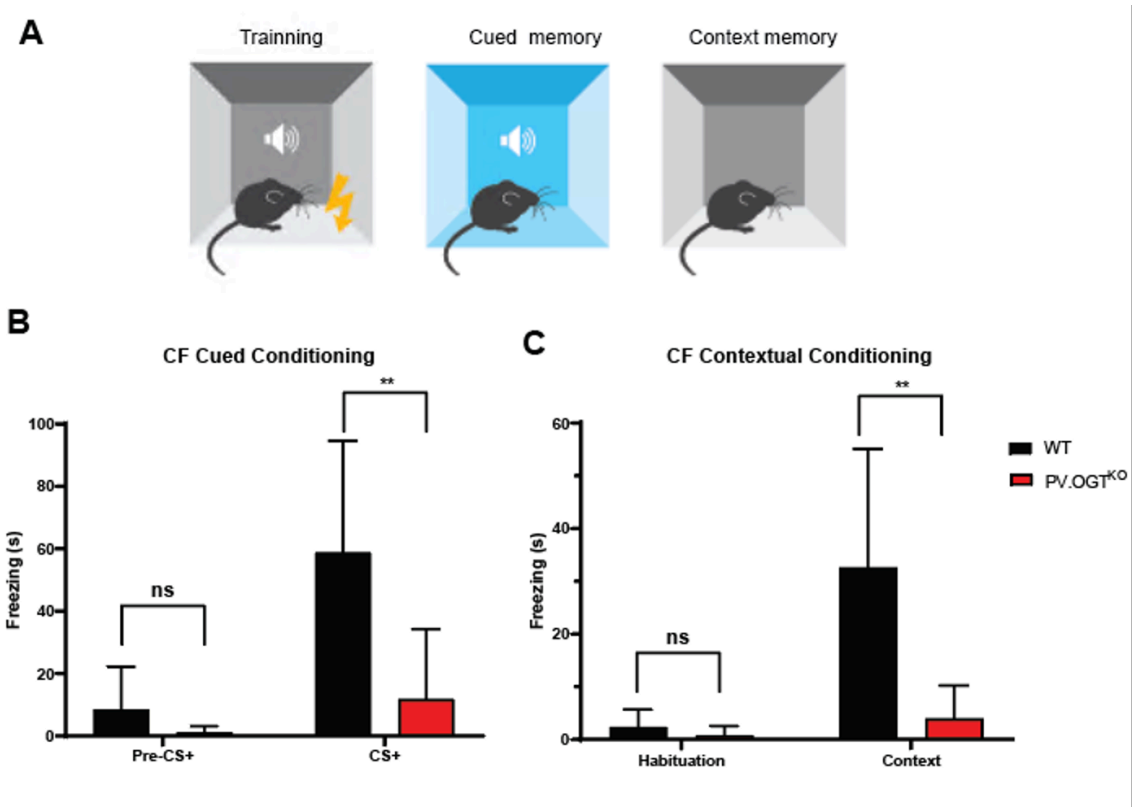

Supplemental Figure 2.1: (A)Schematic of fear condition training. (B) Fear conditioning results quantified as time freezing. No significant difference was found between any groups in freezing to a novel context or a tone stimulus in a pre- conditioned stimulus (pre-CS+). However, conditional stimulus with cued conditioning was significant as KO mice freeze less.(C)After contextual conditioning PV.OGTKO mice d learn context memory. Data was analyzed with one-way ANOVA with a Sidak's multiple comparisons test. Graphs show means ± SD, n=5-6 animals per condition at each dose. Mice were at 5-weeks of age. **P<0.005.

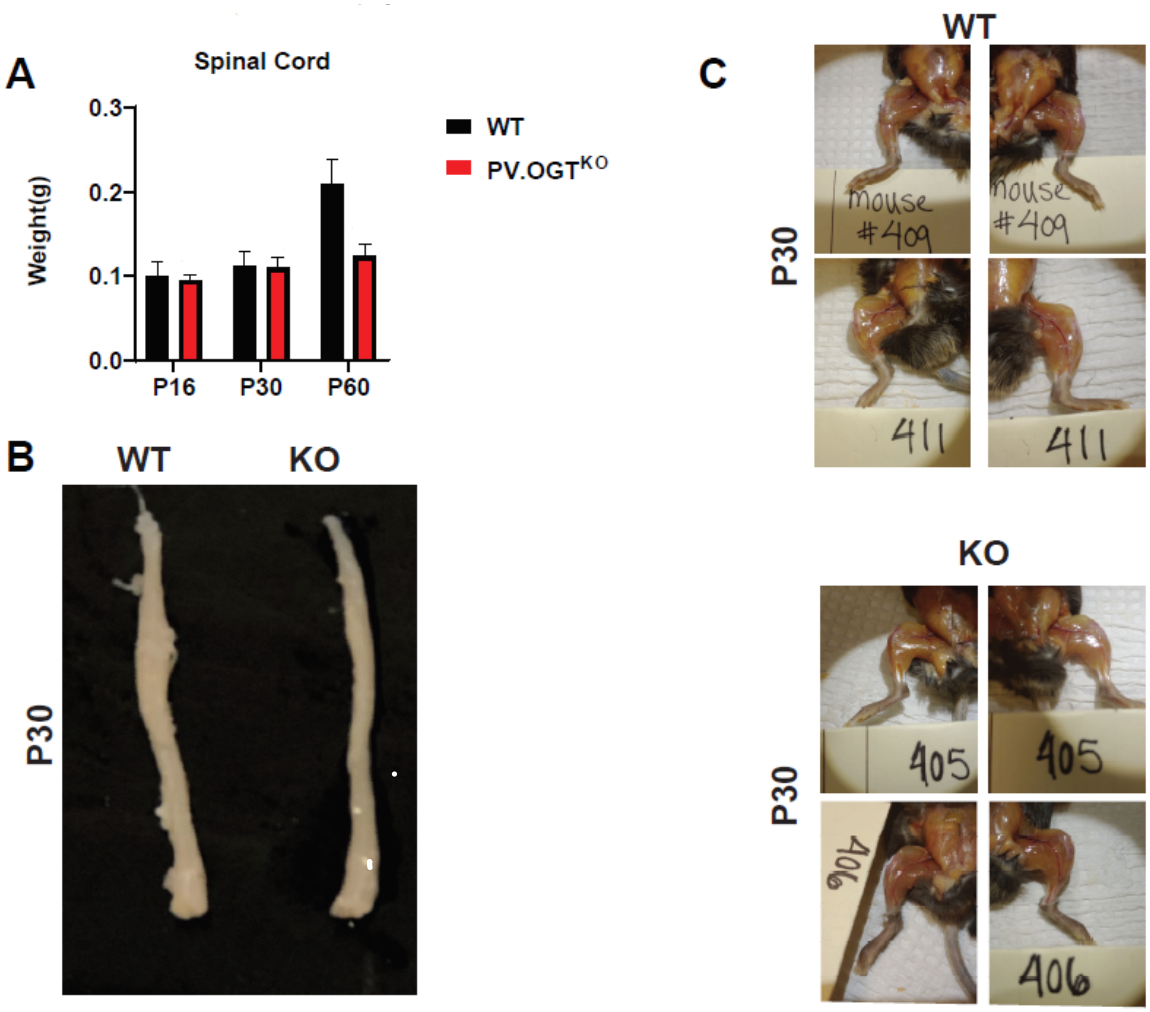

Supplemental Figure 2.2: Spinal and muscle tissue images. (A) reduced in spinal tissue mass in KO mice from P16-P30. (B) image displaying spinal tissue of WT and KO mice at P30.Deletion of OGT in PV neurons shows KO mice spinal tissue shrinkage. (C) Muscle tissue image before extraction at P30 of KO and WT. KO mice show minor muscle atrophy. Mice at P16 WT (n=3), KO (n=2), mice at P30 WT (n=4), KO (n=3), and mice at P60 WT (n=2), KO (n=3).

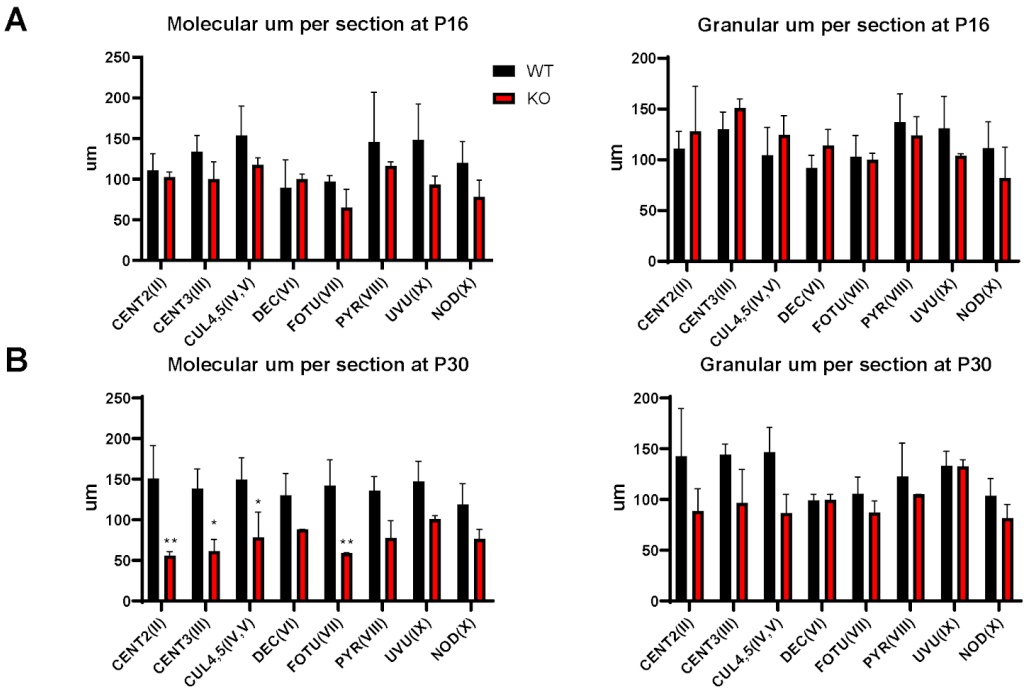

Supplemental Figure 2.3:At P30 PV.OGT KO mice have a reduction in molecular layer width compared to granular layer. (A)No significant finding of layer width measurement at P16. (B) Only a few lobes were reduced in width in the molecular layers on KO mice (CENT2, CENT3, CUL4,5, and FOTU). Three sections were analyzed per mouse (n=1). Data analysis was performed using Sidak's multiple comparisons test. **p<.001, *p<.03.

A

Tissue	E 14-19.5	P 0-21	Adult >P 43
Cerebellum	√	√	√
Cerebral cortex			√
Hippocampus			√
Hypothalamus			√
Thalamus		√	√
Skeletal muscle		√	√

B

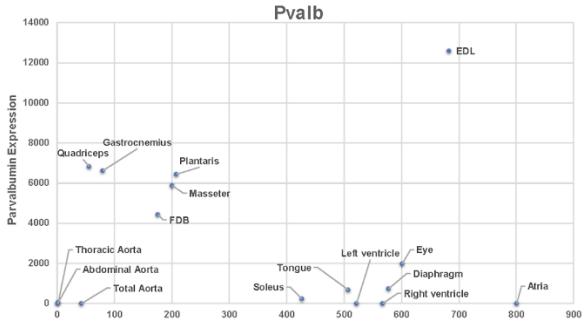

Supplemental Figure 2.4: (A) Cre-expression age depended in different brain regions. (B) Parvalbumin- RNA expression in different muscle tissue, Extensor digitorum longus (EDL) has the highest level compared to others.

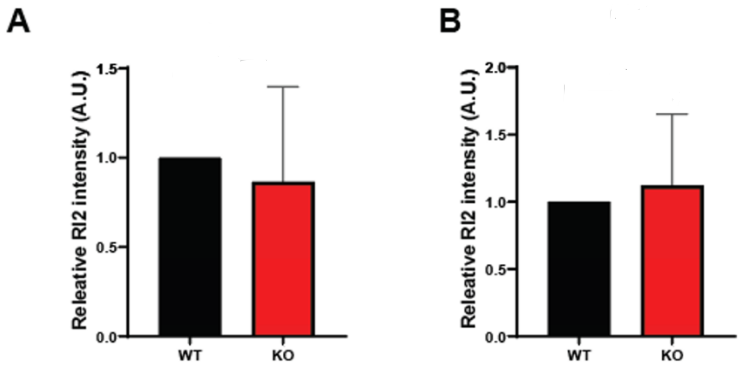

Supplemental Figure 2.5: O-GlcNAc levels measurements in non-PV neurons. (A)(B) no significant findings in O-GlcNAc level changes in other neurons and glia of Cortex (secondary somatosensory) and CA1 (70-50 cells counted) (n=2).

Supplemental Table 2.1:

Cell-type specific OGT KO phenotypes in the nervous system.

Paper	Author	Transgenic mice genotypes	Age phenotype starts	Analyzed nervous system region
Loss of O-GlcNAc glycosylation in forebrain excitatory neurons induces neurodegeneration.	Wang, A. C., et al	OGT-cKO (OGTflxαCamKII-Cre)	P 14-21	Cortex, hippocampus, caudate nucleus, thalamus, and hypothalamus.
The nutrient sensor OGT in PVN neurons regulates feeding.	Lagerlöf, O., et al	αCaMKII-CreER^{+} × OGT$^{Fl/WT}$ × TdT^{Fl}	P 40-70	Hypothalamus PVN
Schwann cell O-GlcNAcylation promotes peripheral nerve remyelination via attenuation of the AP-1 transcription factor JUN.	Kim, S., et al.	OGT-SCKO (P_0-Cre, Ogt^{loxP})	P 40	PNS
Schwann Cell O-GlcNAc Glycosylation is required for Myelin Maintenance and Axon Integrity	Kim, S., et al.	OGT-SKO (P_0-Cre, Ogt^{loxP}) *Prx*	P 60-90	PNS
O-GlcNAc Transferase Is Essential for Sensory Neuron Survival and Maintenance.	Su, C., et al	*Nav1.8-Cre$^{-/+}$ Ogt$^{loxP/Y}$* *brn3a-CreER$^{T2-/+}$ Ogt$^{loxP/Y}$*	P 1 P 50 (induced)	DRG sensory neurons

MATERIALS AND METHODS

Mice

Age-matched (P16, P30, P90) male C57Bl/6J mice were housed at 22-24°C using a 12h light/12h dark cycle with ad libitum access to standard mouse chow and water. Care of animals and diet change procedures were approved by the BNH vivarium and use Committee.

Behavioral Evaluation

All behavioral tests were performed at the Scripps core by Dr. Amanda Roberts. Mice were transferred at either between 3-4weeks of ages, 5-WT mice and 6-KO-mice, and 11-12 weeks of age, 4-WT mice and 4-KO mice. In additional, all animals were sacrificed at the Scripps core after all the behavioral assessments were performed which took 2-3 weeks after initial transfer.

Health/Neuroscreen Test.

This simple test allows for the examination of general health and behaviors in mice and is sensitive to changes in self-care, increases in distress/stress, and illness. The first few measures are taken by observing each mouse in its home cage prior to any handling. These included an examination of coat condition, a check for barbered hair, piloerection, body tone, skin color, and limb tone. The home cage behavior prior to cage opening is also noted (i.e. solitary sleeping, nesting) and any evidence of fighting or aggression is noted. The mouse is petted while still in the cage and it is noted if the mouse moves away. Then the mouse is lifted by its tail and its behavior examined for passivity, trunk curl, and forepaw reaching. The mouse is scruffed for a firm hold and struggling and vocalization are noted. While scruffed, eye blink, ear twitch, whisker and toe pinch

reflexes are assessed. The muzzle is examined for missing whiskers. A dowel is placed in front of the muzzle and biting behavior is scored. The mouse is then released onto a wire cage top. The top is slowly rotated so that the mouse is clinging upside down (if it is able) and time to fall is recorded. Finally, the mouse is placed in an empty, clean cage and freezing on transfer, wild running and stereotypies are noted, if any. Cage exploration is scored. Finally, the mouse is weighed and then returned to its home cage.

Hanging Wire Test.

Mice will be held so that only their forelimbs contact an elevated metal bar (3 mm diameter, 37 cm above the floor). Each mouse will be given three trials separated by 30 seconds. Each trial is scored as follows: 0 — fell off, 1 — hung onto the wire by two forepaws, 2 — hung onto the wire by two forepaws, but also attempted to climb onto the wire, 3 — hung onto the wire by two forepaws plus one or both hindpaws around the wire, 4 — hung onto the wire by all four paws plus tail wrapped, 5 — escaped. Latency to falling off will be measured up to a maximum of 30 s.

Grip strength Test.

Muscle strength is measured in the fore limbs and hind limbs using a dual digital grip strength meter with mesh pull bars from Columbus Instruments. To measure the grip strength, the mouse is allowed to grip the instrument grid with all four paws. Then, the mouse will gently and steadily be pulled back until the grip is released, at which moment the maximal grip strength is recorded by the instrument. This procedure will be repeated

3 times per animal and the average of the two highest forces (in Newtons) will be calculated.

EchoMRI Test.

The EchoMRI 3-in-1 instrument (EchoMRI LLC, Houston, TX) is a quantitative nuclear magnetic resonance (qNMR) imaging system for whole body composition analysis of anaesthetized small animals [23, 24], and qNMR body composition analysis with EchoMRI instrumentation has been proposed to be "gold standard" methodology for metabolic studies in the mouse [25]. Following calibration, each mouse was placed in a holder and placed into the EchoMRI chamber and lean mass, fat mass and water mass were calculated.

Open Field Test.

This test examines general activity, reaction to novelty, and anxiety-like behavior [26]. The mouse is placed in a brightly lit (400 lux) white Plexiglas open arena (50 x 50 x 39cm) and its activity is monitored by a video camera mounted directly over the test arena. Each animal is placed in the center of the field and several behavioral parameters (distance traveled, velocity, center time, frequency in center) is recorded during a 10-minute observation period and analyzed using Noldus Ethovision XT software.

Cued and contextual fear conditioning.

In this procedure, mice learn to associate a novel environment (context) and a previously neutral stimulus (conditioned stimulus, a tone) with an aversive foot shock stimulus [27].

It allows for the assessment of both hippocampus-dependent and hippocampus-independent learning processes in the same mouse [28, 29]. Testing then occurs in the absence of the aversive stimulus. Conditioned animals, when exposed to the conditioned stimuli, tend to refrain from all but respiratory movements by freezing. Freezing responses can be triggered by exposure to either the context in which the shock was received (context test) or the conditioned stimulus (CS+ test). Conditioning takes place in Freeze Monitor chambers (Med Associates, Inc.) housed in sound proofed boxes. The conditioning chambers (26 x 26 x 17 cm) are made of Plexiglas with speakers and lights mounted on two opposite walls and shockable grid floors.

Staining and fixing

Histological analysis with immunofluorescence

Mice were transcardially perfused with cold 4% (wt/vol) paraformaldehyde (PFA) and were fixed overnight in 4% (wt/vol) PFA at 4 °C, followed by three 10 minutes washes with PBS. Sagittal sections (50 μm) were obtained using a Leica VT 1000s and were stored in an PBS solution at −20 °C. Slices were blocked with 5% (vol/vol) goat serum, 0.1% Triton-X 100 in PBS for one hour, washed 3 times (10 minutes) with PBS, and stained with primary antibody in 1% (vol/vol) goat serum, 0.1% Triton-X 100 in PBS overnight at 4 °C. The secondary (DF:1500) was applied the following day (1-2hrs) at room temperature. Slices were mounted Southern Biotech DAPI Fluoromount-G (C0100-20), coded, and imaged with a Zeiss LSM 780 confocal microscope, with the investigator blind to the genotype. Images were collected from slices spaced 50 μm apart through the region of interest. A minimum of 2-3 slices was quantified for each animal, and a minimum of 2-4 animals were evaluated for each genotype.

Data Analysis

The quantification of neuron PV expression was based upon 2 criteria. Primarily from cell intensity, measured through Image J using the freehand selection tool. This standardized wildtype intensity influenced the PV-OGT knockout cell consideration, only if they were in the range of the wildtype count. Cell intensity for the wildtype was then determined through GraphPad's nonlinear regression analysis and the creation of histograms. The second criteria for quantification of cells involved the use of DAPI in the general staining of cell nuclei, an overlap of channels was useful in determining whether a PV stain had additional nuclei stain, determining cell component criterion.

In the case of specific brain regions, the MO somatomotor area of the cortex was quantified only at a region of interest (ROI), where the cell count was normalized per area. For the Hippocampus, cells were quantified in regions (CA1, CA2, CA3 and Dente Gyrus), although the area was not taken into consideration, this was done in terms of cell development and migration analysis. Cerebellar PV counts consisted of Purkinje cell counts between the molecular and granular layers. The length of cerebellar lobes was also taken using selection tools and measurements on Image J, starting from lobe II-X.

REFERENCES

[1] Mergenthaler P, Lindauer U, Dienel GA, Meisel A. Sugar for the brain: the role of glucose in physiological and pathological brain function. *Trends Neurosci*. 2013;36(10):587-597. doi:10.1016/j.tins.2013.07.001

[2] Ackermann RF, Finch DM, Babb TL, Engel J Jr. Increased glucose metabolism during long-duration recurrent inhibition of hippocampal pyramidal cells. *J Neurosci*. 1984;4(1):251-264. doi:10.1523/JNEUROSCI.04-01-00251.1984

[3] Kann, Oliver et al. "Highly energized inhibitory interneurons are a central element for information processing in cortical networks." Journal of cerebral blood flow and metabolism : official journal of the International Society of Cerebral Blood Flow and Metabolism vol. 34,8 (2014): 1270-82. doi:10.1038/jcbfm.2014.104

[4] McCasland JS, Hibbard LS. GABAergic neurons in barrel cortex show strong, whisker-dependent metabolic activation during normal behavior. J Neurosci. 1997;17:5509–5527

[5] Zachara N, Akimoto Y, Hart GW. The O-GlcNAc Modification. 2017. In: Varki A, Cummings RD, Esko JD, et al., editors. Essentials of Glycobiology [Internet]. 3rd edition. Cold Spring Harbor (NY): Cold Spring Harbor Laboratory Press; 2015-2017. Chapter 19. Available from: https://www.ncbi.nlm.nih.gov/books/NBK453063/ doi: 10.1101/glycobiology.3e.019

[6] Wang, A. C., Jensen, E. H., Rexach, J. E., Vinters, H. V. & Hsieh-Wilson, L. C. Loss of O-GlcNAc glycosylation in forebrain excitatory neurons induces

neurodegeneration. Proc. Natl. Acad. Sci. U. S. A.(2016). doi:10.1073/pnas.1606899113

[7] Lagerlöf O, Slocomb JE, Hong I, et al. The nutrient sensor OGT in PVN neurons regulates feeding. Science. 2016;351(6279):1293-1296. doi:10.1126/science.aad5494

[8] Kim S, Maynard JC, Strickland A, Burlingame AL, Milbrandt J. Schwann cell O-GlcNAcylation promotes peripheral nerve remyelination via attenuation of the AP-1 transcription factor JUN. Proc Natl Acad Sci U S A. 2018;115(31):8019-8024. doi:10.1073/pnas.1805538115

[9] Kim S, Maynard JC, Sasaki Y, et al. Schwann Cell O-GlcNAc Glycosylation Is Required for Myelin Maintenance and Axon Integrity. J Neurosci. 2016;36(37):9633-9646. doi:10.1523/JNEUROSCI.1235-16.2016

[10] Su, Cathy, and Thomas L Schwarz. “O-GlcNAc Transferase Is Essential for Sensory Neuron Survival and Maintenance.” The Journal of neuroscience : the official journal of the Society for Neuroscience vol. 37,8 (2017): 2125-2136. doi:10.1523/JNEUROSCI.3384-16.2017

[11] Cole, R. N. & Hart, G. W. Cytosolic O-glycosylation is abundant in nerve terminals. *J. Neurochem.*(2001). doi:10.1046/j.1471-4159.2001.00655.x

[12] Francisco, Herb et al. “O-GLcNAc post-translational modifications regulate the entry of neurons into an axon branching program.” Developmental neurobiology vol. 69,2-3 (2009): 162-73. doi:10.1002/dneu.20695

[13] Liu Y, Li X, Yu Y, et al. Developmental regulation of protein O-GlcNAcylation, O-GlcNAc transferase, and O-GlcNAcase in mammalian brain. *PLoS One*. 2012;7(8):e43724. doi:10.1371/journal.pone.0043724

[14] Wheatley EG, Albarran E, White CW 3rd, et al. Neuronal O-GlcNAcylation Improves Cognitive Function in the Aged Mouse Brain. *Curr Biol*. 2019;29(20):3359-3369.e4. doi:10.1016/j.cub.2019.08.003

[15] 1.Luo, L. *et al.*Optimizing Nervous System-Specific Gene Targeting with Cre Driver Lines: Prevalence of Germline Recombination and Influencing Factors. *Neuron***106**, 37-65.e5 (2020).

[16] Hippenmeyer S, et al., A developmental switch in the response of DRG neurons to ETS transcription factor signaling. PLoS Biol. 2005 May;3(5):e159

[17] Bond, Michelle R, and John A Hanover. "A little sugar goes a long way: the cell biology of O-GlcNAc." The Journal of cell biology vol. 208,7 (2015): 869-80. doi:10.1083/jcb.201501101

[18] Ruan, Hai-Bin et al. "O-GlcNAc transferase enables AgRP neurons to suppress browning of white fat." Cell vol. 159,2 (2014): 306-17. doi:10.1016/j.cell.2014.09.010

[19] Khidekel N, Ficarro SB, Clark PM, et al. Probing the dynamics of O-GlcNAc glycosylation in the brain using quantitative proteomics. Nat Chem Biol. 2007;3(6):339–348. doi:10.1038/nchembio881

[20] Court FA, Coleman MP. Mitochondria as a central sensor for axonal degenerative stimuli. Trends Neurosci. 2012;35(6):364–372. doi:10.1016/j.tins.2012.04.001

[21] Pekkurnaz G, Trinidad JC, Wang X, Kong D, Schwarz TL (2014) Glucose regulates mitochondrial motility via Milton modification by *O*-GlcNAc transferase. Cell 158:54–68. 10.1016/j.cell.2014.06.007

[22] Akimoto Y, Comer FI, Cole RN, et al. Localization of the O-GlcNAc transferase and O-GlcNAc-modified proteins in rat cerebellar cortex. Brain Res. 2003;966(2):194–205. doi:10.1016/s0006-8993(02)04158-6

[23] Taicher GZ, Tinsley FC, Reiderman A, Heiman ML. Quantitative magnetic resonance (QMR) method for bone and whole-body-composition analysis. *Anal Bioanal Chem*. 2003;377(6):990–1002. doi:10.1007/s00216-003-2224-3

[24] Tinsley FC, Taicher GZ, Heiman ML. Evaluation of a quantitative magnetic resonance method for mouse whole body composition analysis. Obes Res. 2004;12(1):150–160. doi:10.1038/oby.2004.20

[25] Argmann CA, Houten SM, Champy MF, Auwerx J. Lipid and bile acid analysis. Curr Protoc Mol Biol. 2006;Chapter 29:. doi:10.1002/0471142727.mb29b02s75

[26] Crawley JN. Behavioral phenotyping of transgenic and knockout mice: experimental design and evaluation of general health, sensory functions, motor abilities, and specific behavioral tests. Brain Res. 1999;835(1):18–26. doi:10.1016/s0006-8993(98)01258-

[27] Maren S. Is there savings for pavlovian fear conditioning after neurotoxic basolateral amygdala lesions in rats?. Neurobiol Learn Mem. 2001;76(3):268–283. doi:10.1006/nlme.2001.4042

[28] Rudy JW, Huff NC, Matus-Amat P. Understanding contextual fear conditioning: insights from a two-process model. Neurosci Biobehav Rev. 2004;28(7):675–685. doi:10.1016/j.neubiorev.2004.09.004

[29] Kenney JW, Gould TJ. Modulation of hippocampus-dependent learning and synaptic plasticity by nicotine. Mol Neurobiol. 2008;38(1):101–121. doi:10.1007/s12035-008-8037-9

ACKNOWLEDGMENTS

I would like to acknowledge Professor Gulcin Pekkurnaz for her support as the chair of my committee. Through multiple drafts, her guidance has proved to be invaluable. I want to thank my committee members, Dr.Glasgow and Dr. Jin, for their support as well.

Chapter 2 is co- authored with Roberts, Amanda and De-lugo, Arlina. The thesis author, Norah Al-Azzam, was the primary and first author of this chapter.